GEO Newsletter

Group for Earth Observation

Group for Earth Observation

No 73 - March 2022

This image of Tonga, acquired by Landsat-8 in May 2021, shows the island as it was prior to the explosion of the uninhabited volcanic island Hunga Tonga-Hunga Ha'apai in mid-January 2022.

GEO MANAGEMENT TEAM

General Information

John Tellick,

email: information@geo-web.org.uk

GEO Newsletter Editor

Les Hamilton,

email: geoeditor@geo-web.org.uk

Technical Consultant (Hardware)

David Simmons

email: tech@geo-web.org.uk

Webmaster and Website Matters

Vacancy

e-mail: webmaster@geo-web.org.uk

Management Team

David Anderson

Rob Denton

Nigel Evans: nigel.m0nde@gmail.com

Clive Finnis

Carol Finnis

Peter Green

David Simmons

David Taylor

Useful User Groups

Weather Satellite Reports

This group provided weekly reports, updates and news on the operational aspects of weather satellites.

https://groups.io/g/weather-satellite-reports

SatSignal

This end-user self help group is for users of David Taylor's Satellite Software Tools, including the orbit predictor WXtrack, the file decoders GeoSatSignal and SatSignal, the HRPT Reader program, the remapper GroundMap, and the manager programs - MSG Data Manager, GOES-ABI Manager, AVHRR Manager etc.

https://groups.io/g/SatSignal

MSG-1

This forum provides a dedicated area for sharing information about hardware and software for receiving and processing EUMETCast data.

https://groups.io/g/MSG-1

GEO-Subscribers

This is the official group is for subscribers of the Group for Earth Observation (GEO), aimed at enthusiasts wishing to exchange information relating to either GEO or Earth Observation satellites.

https://groups.io/g/GEO-Subscribers/

Follow GEO on Twitter and Facebook

Group for Earth Observation

Receive the latest news from EUMETSAT, ESA, NOAA, NASA, and the Met Office etc. through their Twitter feeds ...

https://twitter.com/geo_earth_obs

Visit GEO on facebook and link to dozens of news items from NOAA, NASA, ESA, EUMETSAT and much more ...

http://www.facebook.com/groupforearthobservation

From the Editor

Les Hamilton

What a winter Europe has experienced since the December issue. Not so much freezing cold with drifting snow, but milder and very windy. In Scotland, where I live, the combined actions of storms Alex, Corrie, Malik, Dudley and Eunice have caused damage unheard of since that fateful 1953 storm. It is estimated that in excess of eight million mature trees were felled and sawmills throughout Scotland are working round the clock to process all the timber. Northeast Scotland was worst hit, losing over one million trees, some of which actually snapped in half rather than being uprooted!

Looking on the brighter side, we have some great articles for you. Ed Murashie continues his series on the Landsat Earth Observation satellites and details how their instrumentation has developed since the first launch in 1962, exactly 50 years ago. There is more to learn about processing the EUMETCast SAF products as Richard Osborne completes his treatise by including products omitted last issue.

Early this year I was contacted by Ernst Lobsiger, a Swiss EUMETCast enthusiast. Ernst is a physicist and mathematician, and was enthused by Richard Fairman's article in December on overlaying Bracknell MSLP charts on Meteor 2M GIS imagery. He reasoned that it should be possible to digitise the Bracknell MSLP charts and modify them by GIS, thus enabling them to be overlaid accurately on MeteorGIS images. After several weeks of testing the job was done. I've compiled a short note about this, with some illustrations on page 11, and provide a link to a web page I have constructed detailing the technique as I successfully followed Ernst's instructions.

Contents

Storm Eunice, imaged by NASA's Aqua satellite at 12.45 UT on February 17, 2022 as it approached England, bringing the threat of damaging winds of over 150 kilometres per hour.

Larsen B Embayment Breaks Up

NASA Earth Observatory

Story by Kathryn Hansen

After more than a decade fastened to the coastline, a large expanse of sea ice has broken away from the Antarctic Peninsula. The ice, which had persisted in the Larsen B embayment since 2011, crumbled away over the span of a few days in January 2022, taking with it a Philadelphia-sized piece of the Scar Inlet Ice Shelf.

The Moderate Resolution Imaging Spectroradiometer (MODIS) on NASA's Terra and Aqua satellites acquired these natural-colour images of the embayment and ice shelf. The upper image shows the embayment on January 16, 2022, prior to the break up. The lower image shows the same area on January 26, shortly after the sea ice broke up.

Scientists are still investigating the reason for the breakup, but the early clearing of seasonal sea ice along the Antarctic Peninsula suggests that the austral summer has been warm and wet. Scientist Rajashree Tri Datta of University of Colorado, Boulder, noted that föhn winds, influenced by a large atmospheric river, helped destabilise the ice pack.

The breakup is the latest in a series of notable events in the Larsen B embayment over the past 20 years. Prior to 2002, glacial ice on the Antarctic Peninsula flowed toward the sea and fed into a vast floating ice shelf known as Larsen B. The shelf helped to buttress inland tributary glaciers, pushing back against them and slowing their seaward flow. But in early 2002, the shelf abruptly fractured. With 3,250 square kilometres of ice suddenly gone, the glaciers thinned and flowed more quickly into the open water.

Following the collapse of Larsen B, landfast sea ice grew atop the seawater each winter and melted away entirely in most summers.

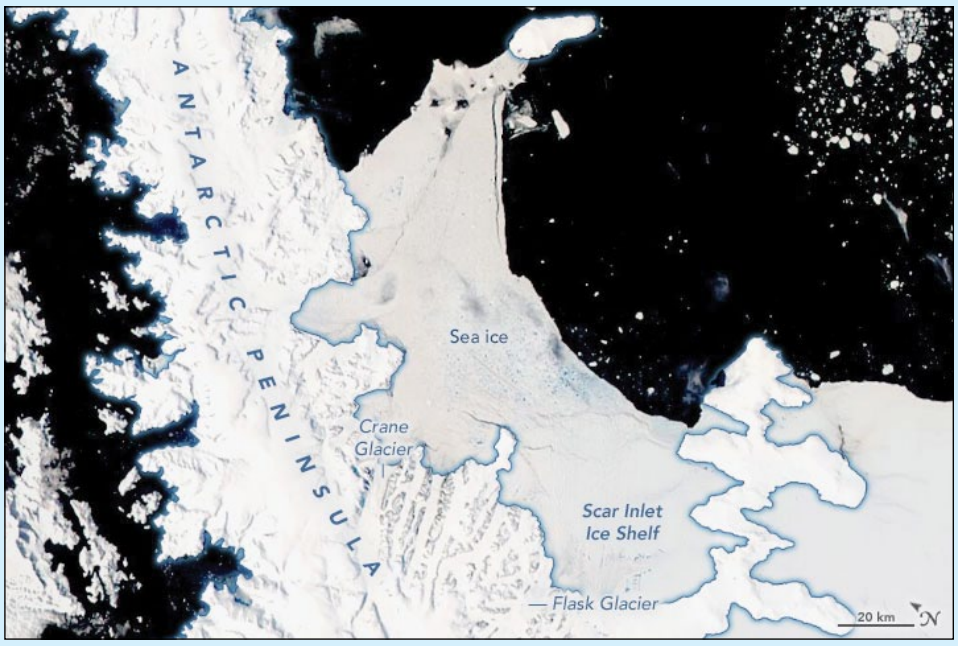

The intact Larsen-B embayment, imaged on January 16, 2022.

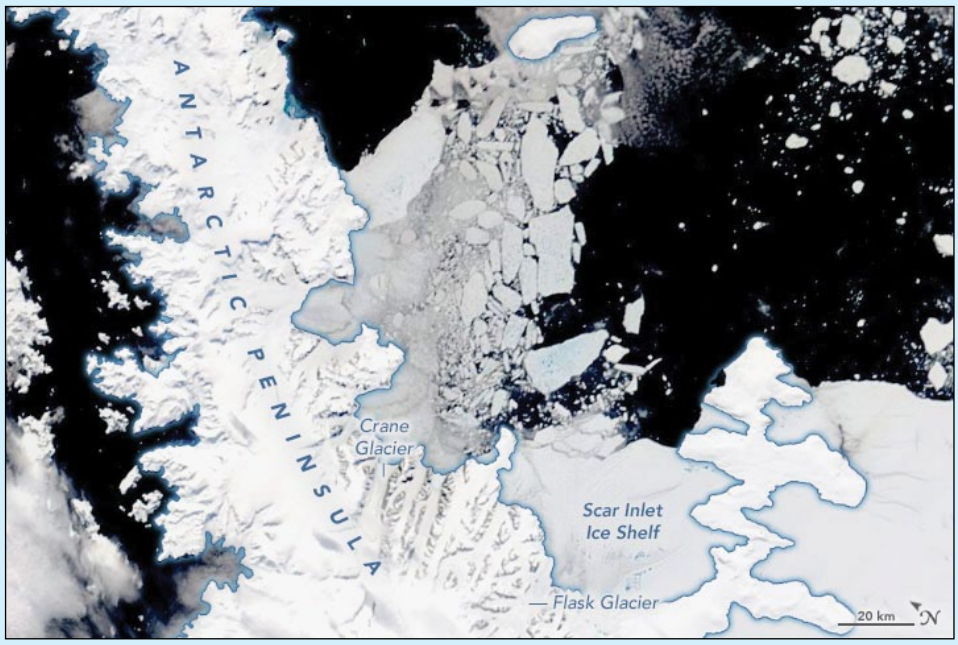

The same area, imaged on January 26, 2022 shortly after breaking up.

But the sea ice that started to grow in late March 2011 stuck around.

> *'It was the first time since the early 2002 shelf collapse that the Larsen B embayment was seen to freeze up and stay frozen through multiple austral summers,'* said Christopher Shuman, a NASA/UMBC glaciologist.

The sea ice retreated slightly at its edges during summers, and its surface occasionally became coated with blue meltwater, but the ice persisted until this January.

Satellite images of the often-cloudy region indicate that the breakup occurred between January 19-21, 2022. Sea ice splintered and floated away from

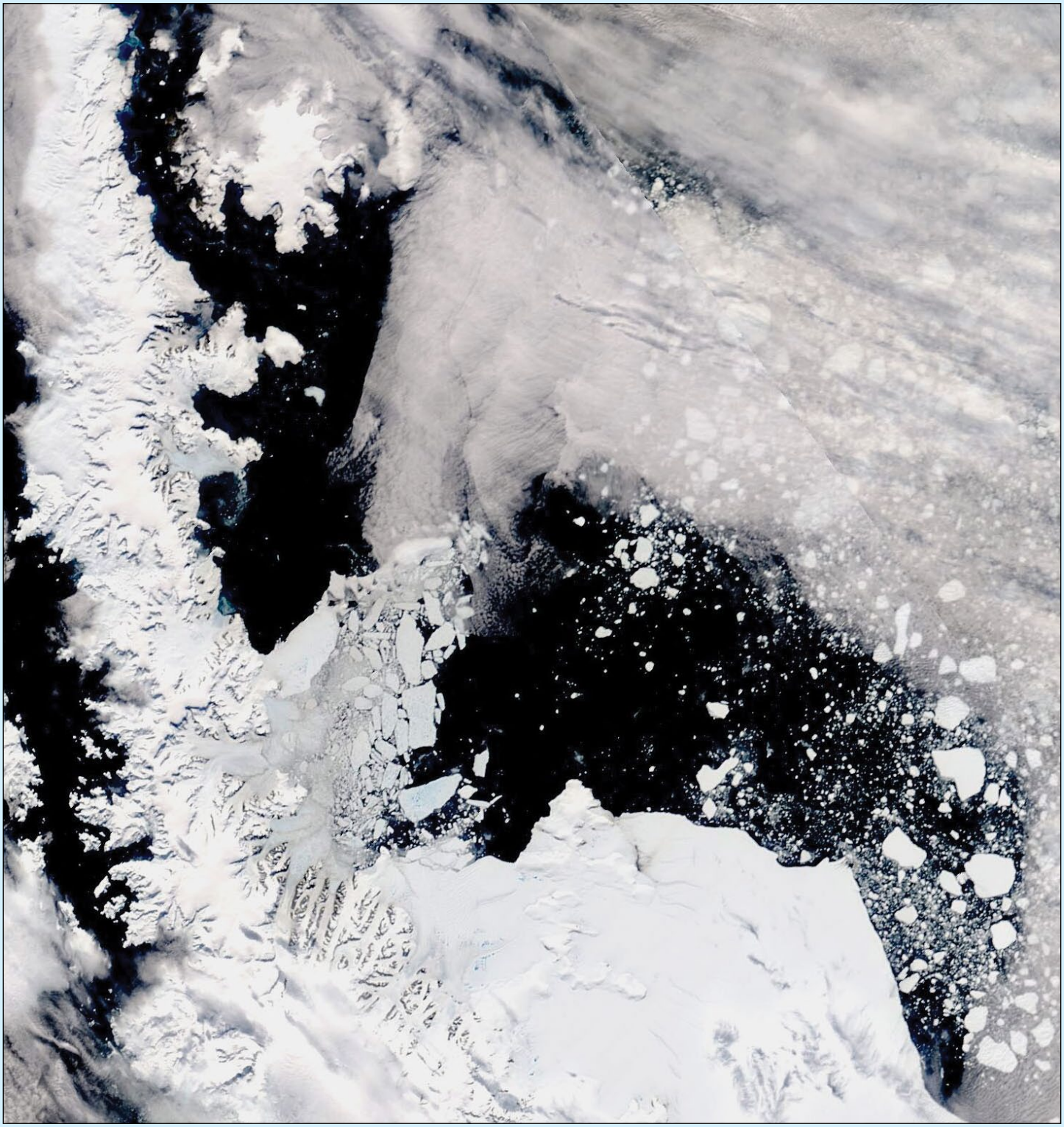

This is a wider view of the Larsen B region shortly after breaking up.

the coast, along with icebergs from the fronts of Crane Glacier and its neighbours to the north and south. Shuman thinks strong outflows of ice from the Flank and Leppard tributary glaciers most likely widened a rift that led the Scar Inlet Ice Shelf—the southern remnant of the Larsen B Ice Shelf—to shed several large icebergs.

Compared to a massive ice shelf (like the original Larsen B), sea ice adjacent to land is less effective at holding back the seaward flow of glaciers, but it still plays a role. This summer's breakup of the sea ice in the embayment is important because—unlike the meltwater from an ice shelf, icebergs, and sea ice (already floating)—the meltwater from a glacier adds to the ocean's volume and contributes directly to sea level rise.

With the sea ice now gone, '*the likelihood is that backstress will be reduced on all glaciers in the Larsen B Embayment and that additional inland ice losses will be coming soon,*' Shuman said.

NASA Earth Observatory images by Joshua Stevens, using MODIS data from NASA EOSDIS LANCE and GIBS/Worldview. .

Island Nation Hit Hard by Eruption

NASA Earth Observatory

Story by Adam Voiland

Ever since the uninhabited volcanic island Hunga Tonga-Hunga Ha'apai exploded in mid-January 2022, the people of Tonga have faced a gauntlet of hazards.

One of the most widespread is volcanic ash. Satellite images collected in the days after the eruption show the fine-grained shards of pulverised rock covering several islands, turning land surfaces from lush green to tan and gray. On January 25, 2022, the Operational Land Imager (OLI) on Landsat-8 captured the image opposite showing ash coating much of Tongatapu, Tonga's most populous island. Compare this with the pre-eruption image featured on the front cover.

The close-up images below show the area near Nuku'alofa before and after the eruption. (Note that the sea water in each image has been masked out in order to focus on land features.)

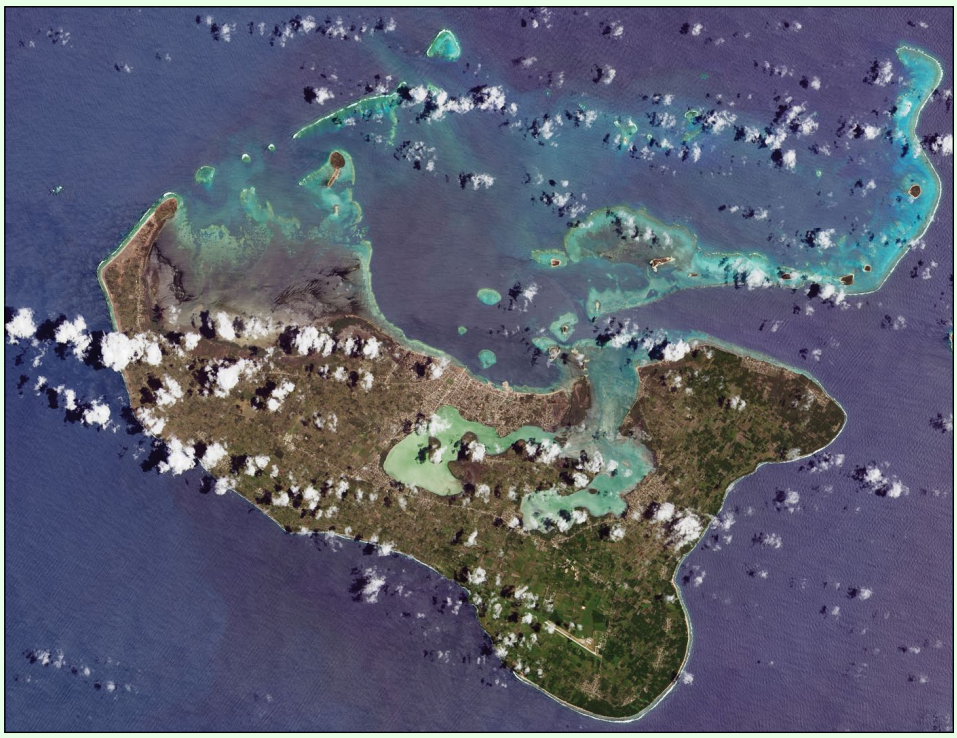

Tongatapu, Tonga's most populous island, imaged by Landsat-8 following the explosion of the Hunga Tonga-Hunga Ha'apai volcano
Image: NASA

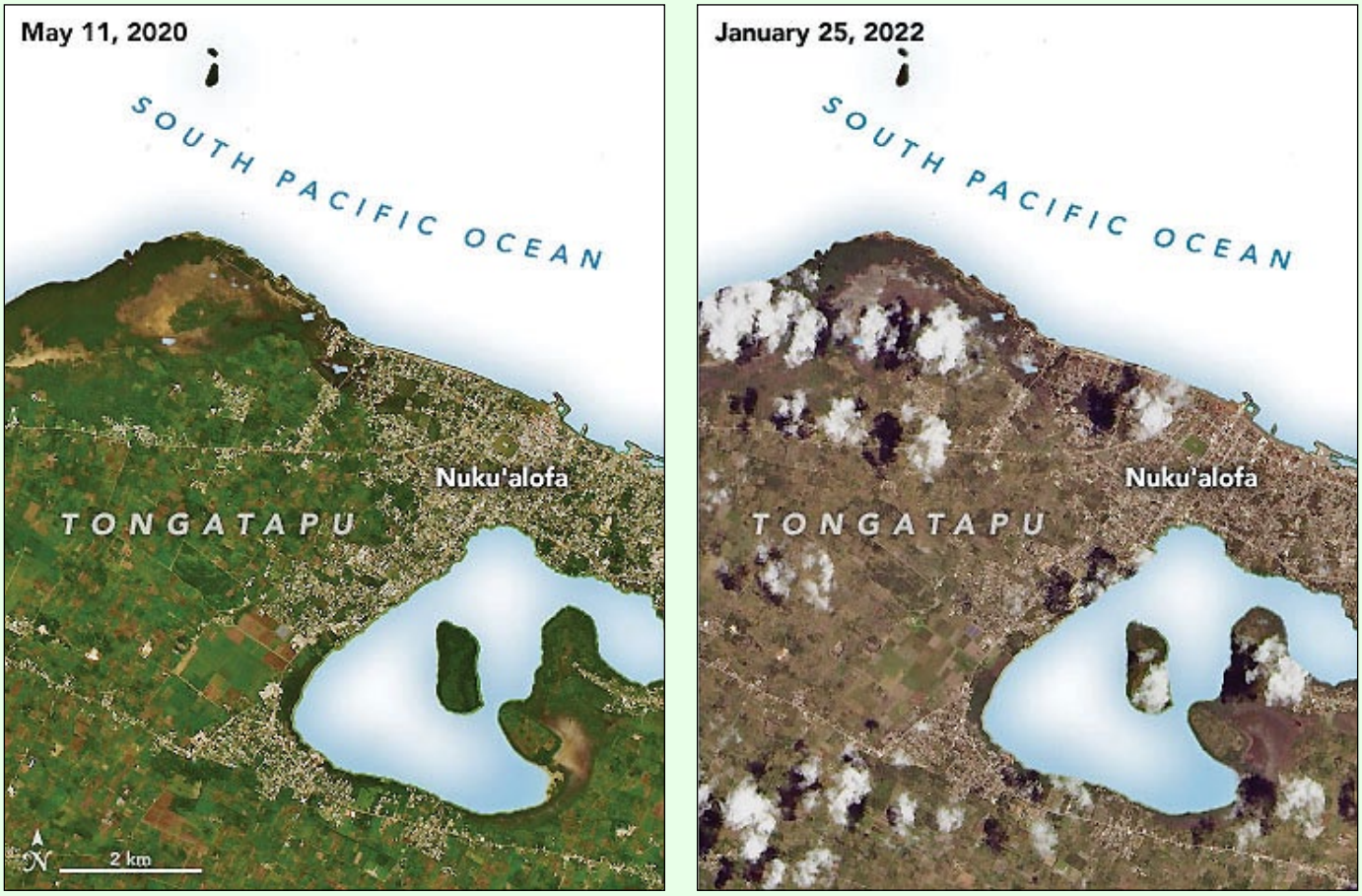

These two images highlight the area near Nuku'alofa, the capital of Tonga, before and after the eruption
Images: NASA

According to the United Nations, an average of two centimetres of ash coated surfaces in the island nation's capital city after the eruption. While the extent of damage from the ashfall is still being assessed, preliminary reports indicate that it had contaminated drinking water, disrupted transportation networks, and most likely damaged crops.

Though it is rare for volcanoes to generate tsunamis, the islands of Tonga were slammed by a series of destructive waves soon after the eruption. Estimates vary, but the Tongan government reported that waves as high as 15 metres may have struck the west coasts of several islands, including Tongatapu and 'Eua. The waves washed away cars and buildings, flattened trees, and damaged power lines on several islands. The United Nations reported that three people were killed and hundreds of buildings were destroyed or damaged by the waves.

After major catastrophes, it's not often clear at first which areas are most in need of aid. Damage proxy maps like the one shown at the top of this page can help governments and first responders gauge where to deploy resources by quickly offering a broad view of possible damages.

The lower damage proxy map shows areas on Tongatapu that were most likely damaged by the eruption and tsunami. Dark red pixels represent the most severe damage, while orange and yellow areas are moderately or partially damaged. Each coloured pixel represents an area of 30 meters by 30 meters (about the size of a baseball infield). Researchers from the The Earth Observatory of Singapore - Remote Sensing Lab (EOS-RS) made the maps by comparing a post-eruption satellite radar image from January 22, 2022, with pre-eruption images from March 2019 and March 2020.

The technique showed an especially severe line of damage along Tongatapu's northern coast. Other hard-hit areas included small islands north of Tongatapu, including Nomuka, Mango, and Fonoifua. One damage assessment from the United Nations Office for the Coordination of Humanitarian Affairs indicates that 100 houses have been damaged or destroyed in Tongatapu.

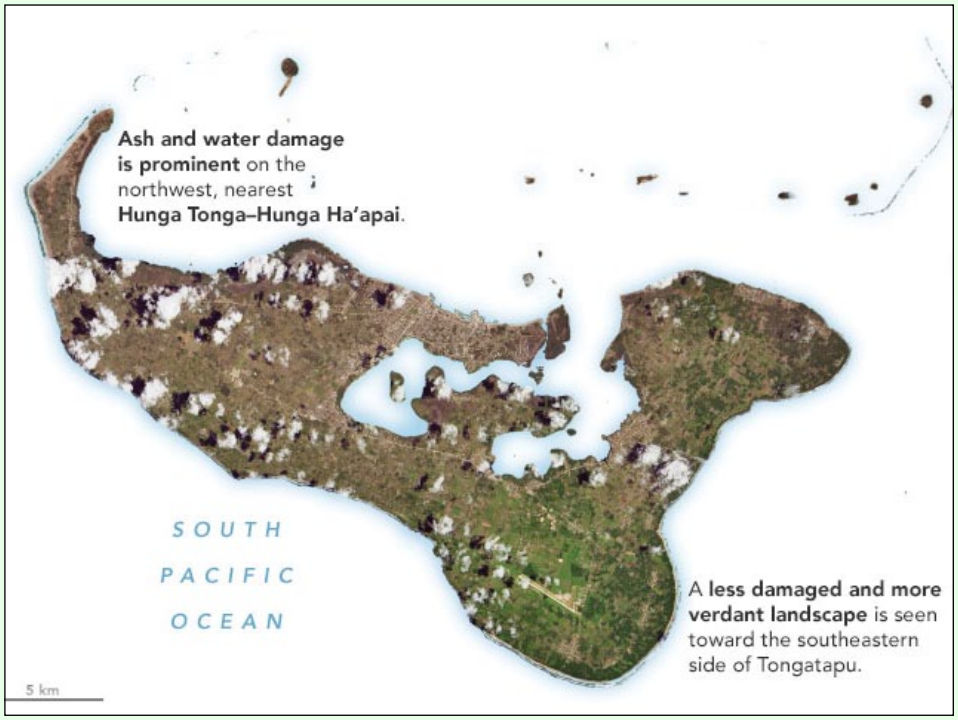

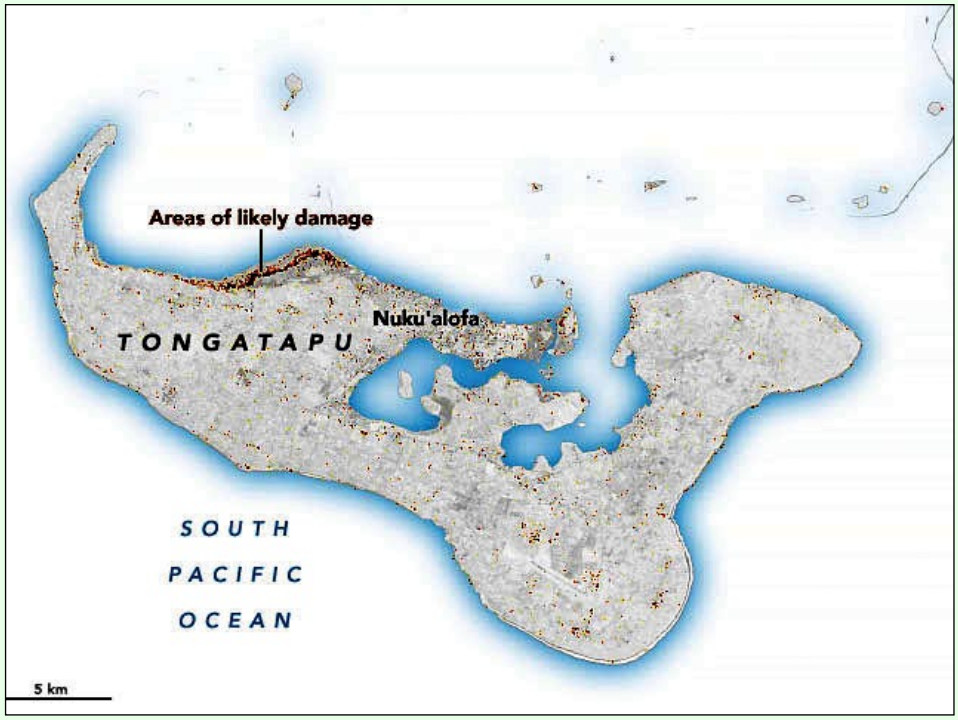

The damage proxy maps were derived from synthetic aperture radar (SAR) images acquired by the Advanced Land Observing Satellite-2 (ALOS-2) satellites, operated by the Japan Aerospace Exploration Agency (JAXA).

SAR instruments send pulses of microwaves toward Earth's surface and observe the reflections of those waves. By comparing signals from before and after an event, researchers can map changes in the land surface and the built environment.

The techniques used for these maps were developed by researchers in the Advanced Rapid Imaging and Analysis (ARIA) group at NASA's Jet Propulsion Laboratory, the California Institute of Technology, and EOS-RS. The ARIA team is supported by NASA's Earth Science Disasters Program.

NASA Earth Observatory images by Joshua Stevens, using Landsat data from the U.S. Geological Survey and ALOS-2 data from the Japan Aerospace Exploration Agency/ JAXA and the Earth Observatory of Singapore Remote Sensing Lab.

Water in Lake Eyre

MODIS Web Image of the Day

https://modis.gsfc.nasa.gov/gallery/showall.php

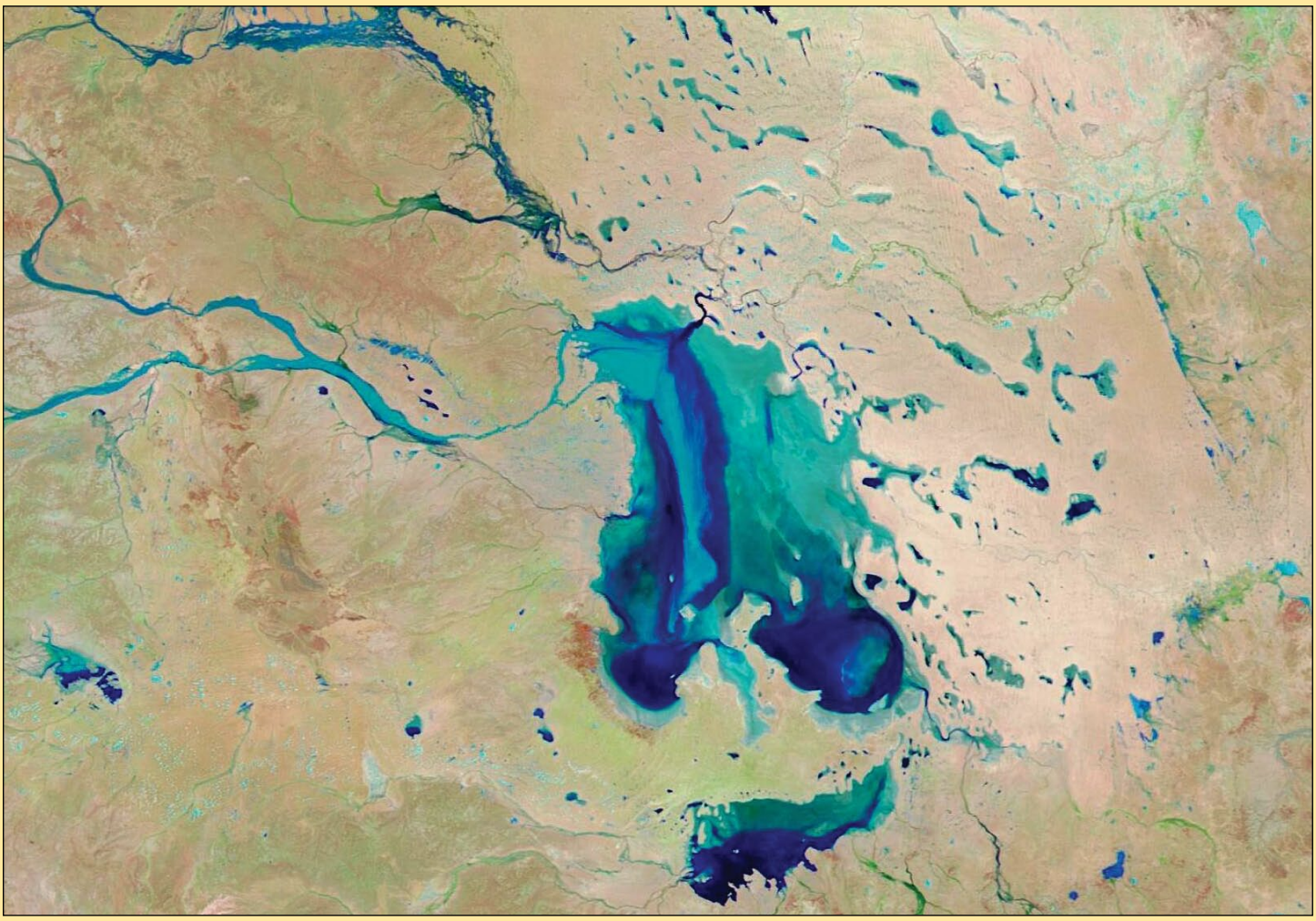

Image Credit: MODIS Land Rapid Response Team, NASA GSFC

Lake Eyre, Australia's largest salt pan, sits in the dry outback about 650 kilometres north of Adelaide in the state of South Australia. Also called Kati Thanda or Kati Thanda-Lake Eyre, the large lake lies 15 metres below sea level in one of the biggest internal drainage systems in the world. The Lake Eyre Basin stretches over southeastern Northern Territory, southwestern Queensland, northwestern New South Wales, and the northeast of South Australia.

Normally the lake is nearly dry and crusted with salt, but when heavy rains fall anywhere across the basin, water often makes it way through rivers and channels to bring at least some moisture to Lake Eyre. Flooding strong enough to fill the lake is rare, but some seasonal filling is not uncommon, especially in the monsoon season, which runs from December through April in much of the Lake Eyre Basin.

Flooding rains struck parts of the Australia outback in late January 2022, followed by heavy storms in South Australia in early February, all adding up to record rainfalls to some areas. While the storms wreaked havoc, washing out roads and flooding highways, the abundant water began to trickle-down to the Lake Eyre Basin.

On February 5, 2022, the Moderate Resolution Imaging Spectroradiometer (MODIS) on board NASA's Terra satellite acquired this false-colour image showing water filling Lake Eyre and the normally dry outback around the lake. The false-colour image is composed from a combination of infrared and visible light (MODIS bands 7-2-1), where water appears dark and light blue; bare ground is brown; and vegetation is bright green. This band combination makes it easier to see where water is present.

According to the National Parks and Wildlife Service South Australia's web page, 'each time the lake floods, the salt crust which forms much of its surface begins to dissolve until the salt level in the water reaches saturation point. When the lake starts to fill, the surface water is fairly fresh and drinkable because the heavier salty water is close to the lake bottom. From the air, water salinity variations can be seen as remarkable swirling current patterns.' Such swirling patterns are visible, especially in the southern portion of Lake Eyre North.

Russia's Crater of Diamonds

NASA Earth Observatory

Story by Kasha Patel

About 36 million years ago, an asteroid slammed into northern Siberia and created one of the largest craters on Earth. Streaking in at an estimated speed of 20 kilometres per second, the asteroid made an impact that ejected millions of metric tons of material into the air. The asteroid—between 5 and 8 km wide—created a crater nearly 100 km in diameter.

Popigai crater is the fourth largest verified impact crater on Earth, tying with the Manicouagan Reservoir in Canada. The three larger craters are either buried (Chicxulub), deformed (Sudbury), or severely eroded and deformed (Vredefort). Popigai has only been slightly modified by erosion, leaving it as one of the most well-preserved craters in the world.

The images on this page show Popigai crater, named for a nearby river. The images were created using Blue Marble data, a cloud-free composite of monthly observations from NASA's Moderate Resolution Imaging Spectroradiometer (MODIS) observations. The data were draped over an ASTER-derived global digital elevation model, which shows the topography of the area.

Located about 100 km from the Laptev Sea coast, the round depression dives about 150 to 200 metres below the surrounding land. Geological mapping and field observations show a central depression at the bottom of the crater, surrounded by a peak ring of about 45 km wide. The ring gradually passes outwards into a ring-shaped trough, which is surrounded by a flat annular terrace.

The crater sits on the northeastern margin of the Anabar shield, which contains a mix of graphite-bearing rocks and sedimentary rocks. The impact from the asteroid melted 1,750 cubic kilometres of rocks and instantly transformed the flakes of graphite into diamonds. Diamonds formed in a hemispherical shell about 1.6 km

Concluded on page 23

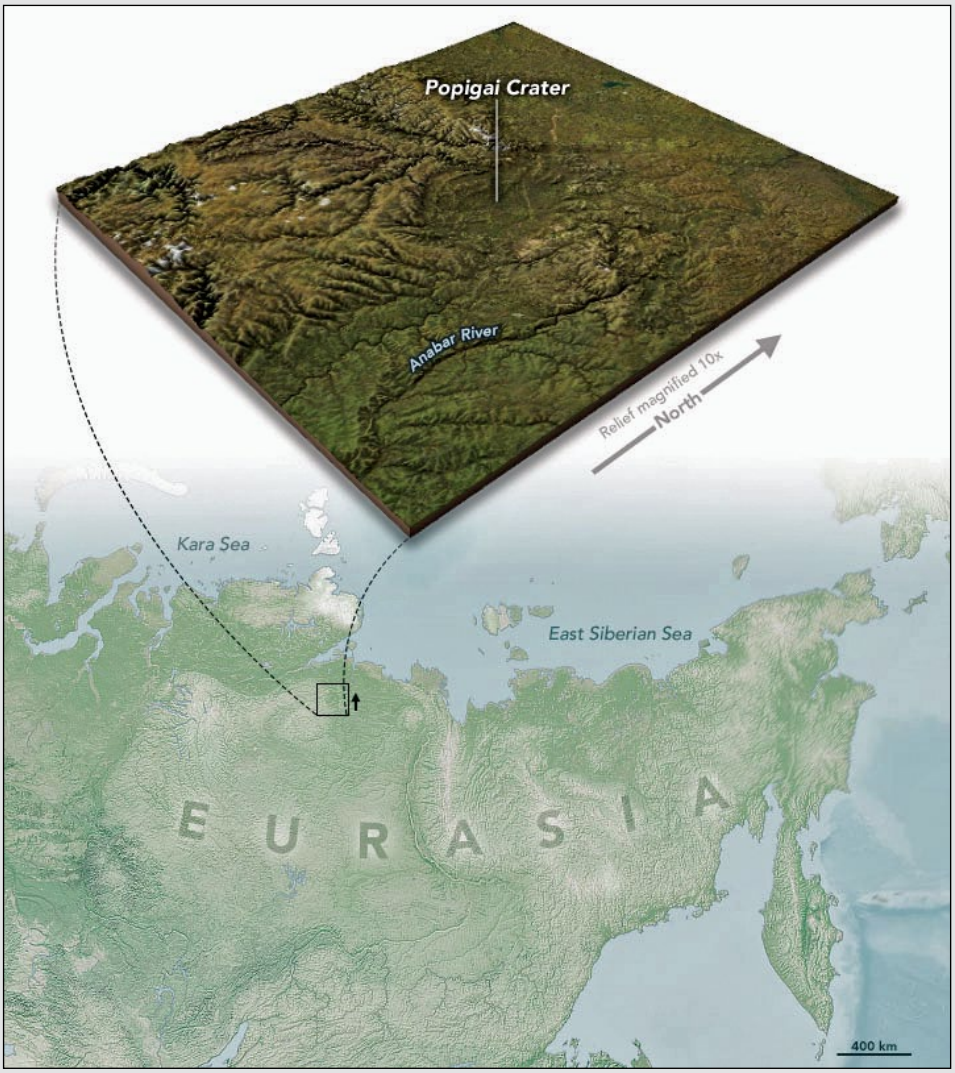

NASA Earth Observatory images by Joshua Stevens, using data from NASA/METI/AIST/Japan Space Systems, and the U.S./Japan ASTER Science Team, and Blue Marble data from NASA Earth Observatory

Using Shapefiles to

Overlay Digitised Bracknell Charts on Meteor M2 Images

Les Hamilton

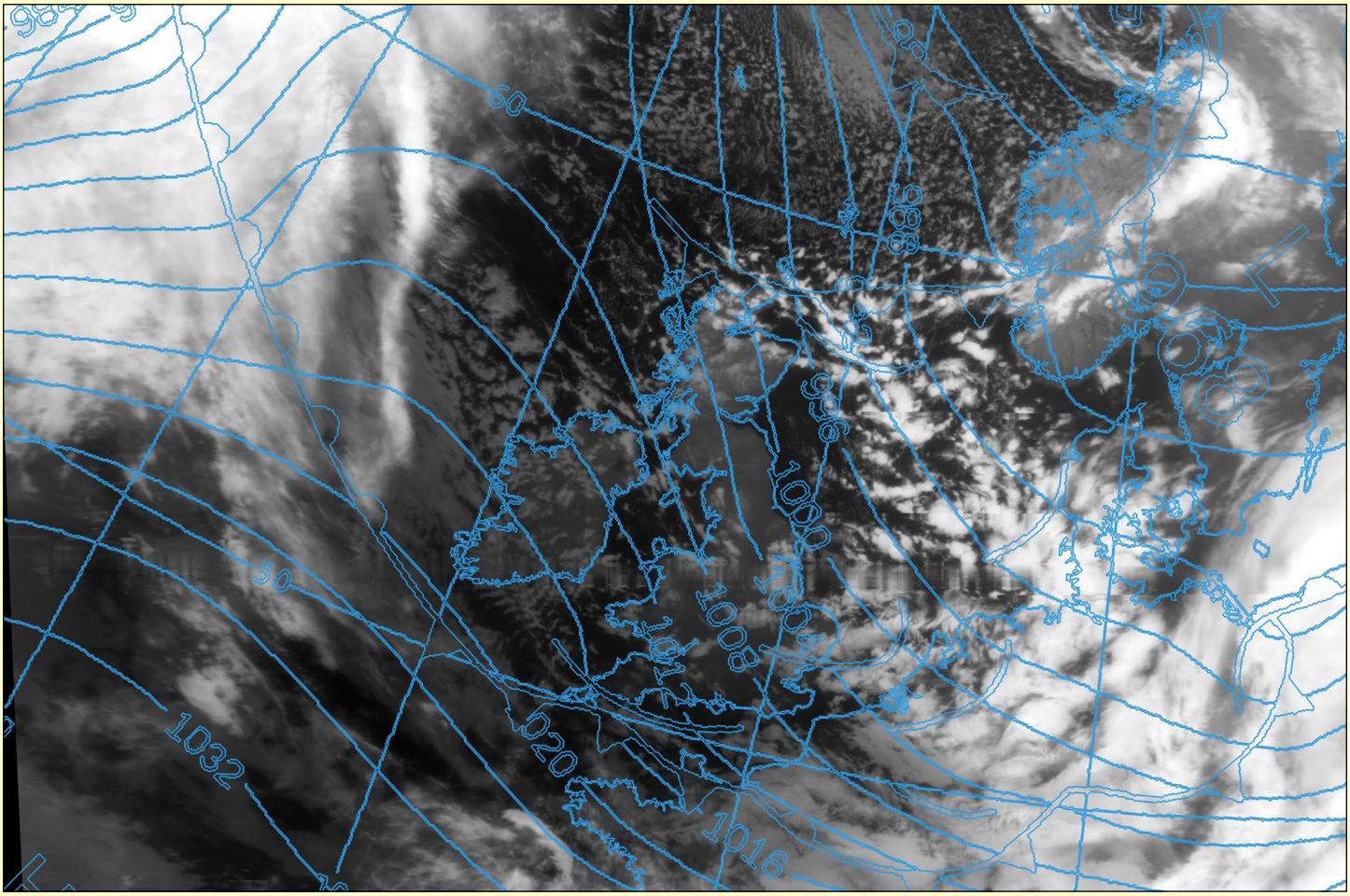

This is a section of a Meteor M2 infrared image was captured at 18.09 UT on February 6 2022 and rendered in MeteorGIS
It is shown bearing the 1800 UTC Bracknell MSLP chart for that day.

Around mid December last year I received an email from Ernst Lobsiger, a Swiss physicist and retired teacher, who had taken a great interest in Richard Fairman's article on overlaying Bracknell MSLP charts [1] on Meteor M2 images. He pointed out, however, that the technique was somewhat approximate as the two entities did not share the same mapping projection. But he believed that he might be able to provide totally accurate overlays by developing shapefiles from the Bracknell charts which the MeteorGIS software itself could then overlay on the Meteor M2 images.

A shapefile [2] is a digital geospatial vector data format for geographic information system (GIS) software, which spatially describes points, lines, and polygons as vector features. The **MeteorGIS.exe** software already uses shapefiles every time it overlays coastlines, country boundaries, the graticule and major cities on your Meteor images. You will find these shapefiles inside the MeteorGIS subfolder with names such as '**ne_50m_coastline**' and '**ne_110m_graticules_10**'. They always exist as file triples with endings .shp (coordinates), .shx (pointers) and .dbf (attributes).

Ernst reasoned that, if he could digitise the full-sized weather charts from *www.weathercharts.org*, it would be possible to create a set of shapefiles that MeteorGIS could draw upon to automatically add accurate MSLP Bracknell charts to Meteor images.

As Ernst does not run a Windows MeteorGIS system (he runs EUMETCast receivers under GNU/Linux), I provided him with a few Meteor M2 S-files with which to carry out his experiments.

Unlike the situation with coastlines etc, which are constant and where the same shapefiles can be used every time, the data contained in Bracknall charts is dynamic: it changes every six hours from one chart to the next. This means that the user requires a means to create a new set of Bracknell shapefiles daily, if not even for each Meteor pass! This is achieved using **QGIS**, a Free and Open Source Geographic Information System tool. Although it takes some time to become fully familiar with all the steps in the process, by the time you have memorised them, a new set of Bracknell Shapefiles can be created from a downloaded chart in no more than a couple of minutes.

Ernst has prepared an instruction/information PDF document describing every detail of the process he has devised, fully illustrated at each step. He has also provided scripts that automatically download and prepare the latest Bracknell charts.

These scripts are far too detailed to reproduce here and, in any case, copying them accurately would be a major undertaking. They can all be downloaded from the following URL

https://leshamilton.co.uk/BracknellGIS.htm

where which I explain how to integrate Ernst Lobsiger's methodology into the MeteorGIS folder itself.

This web page explains my own experiences as I followed Ernst Lobsiger's instructions, and provides links for downloading all the necessary software and scripts. It also explains how to create **Bracknell.bat** and **Bracknell.ini** files to simplify adding the Bracknell shapefiles to your images (and also a link to download them, ready prepared, if you prefer).

References

1 Bracknell Charts
https://www.weathercharts.net/ukmo_mslp_analysis/ppva_fullsize.gif

2 Shapefile
https://en.wikipedia.org/wiki/Shapefile

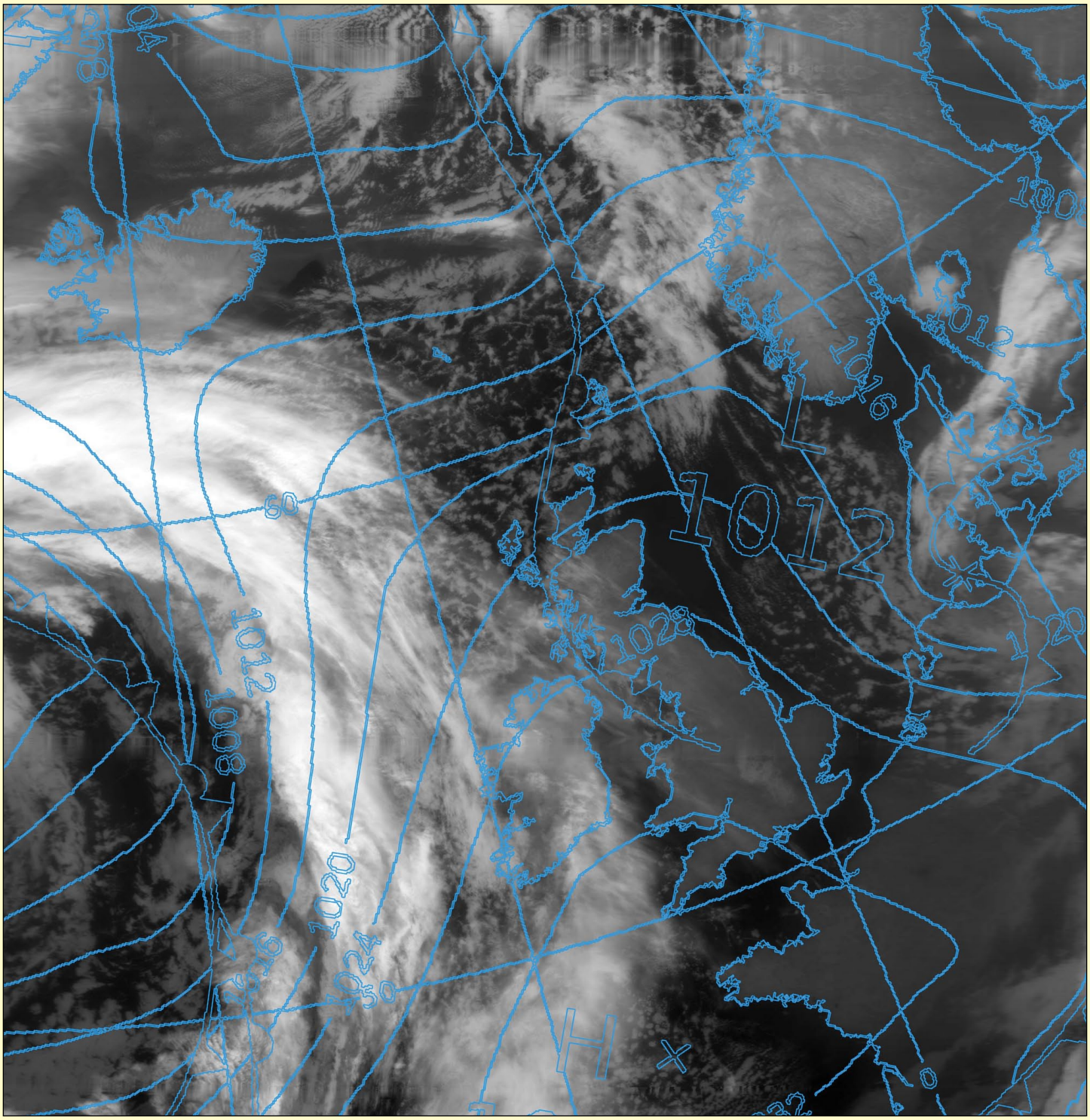

This is a segment from a Meteor M2 infrared image captured at 08.23 UT on February 11, 2022.
It is shown bearing an overlay of the noon Bracknell MSLP chart for that day.

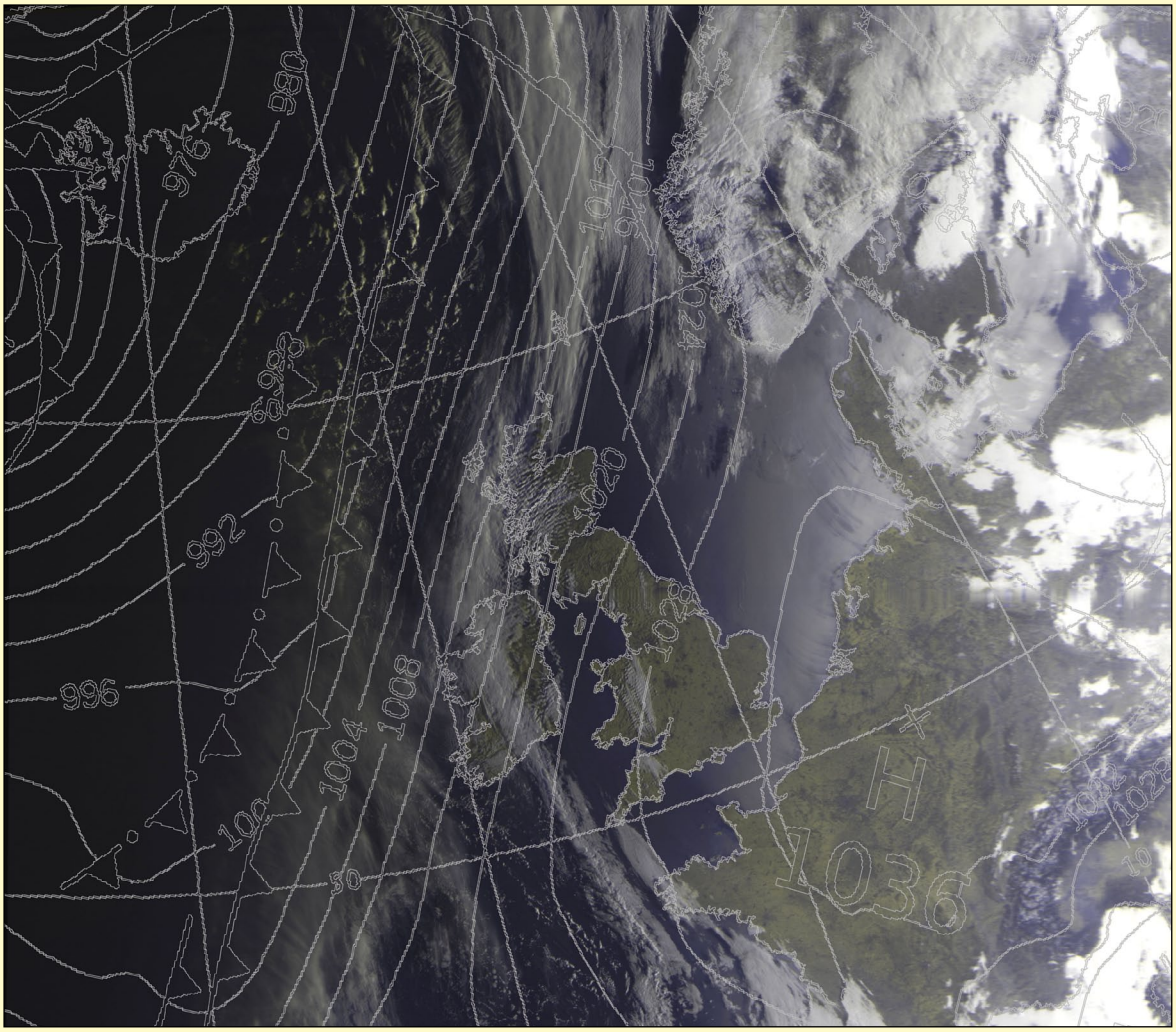

Captured at 08.01 UT on the morning of February 27, 2022, this is the first decent visible image of the year from Meteor M2. The Bracknell overlay shows high pressure advancing from France as a depression builds over Iceland.

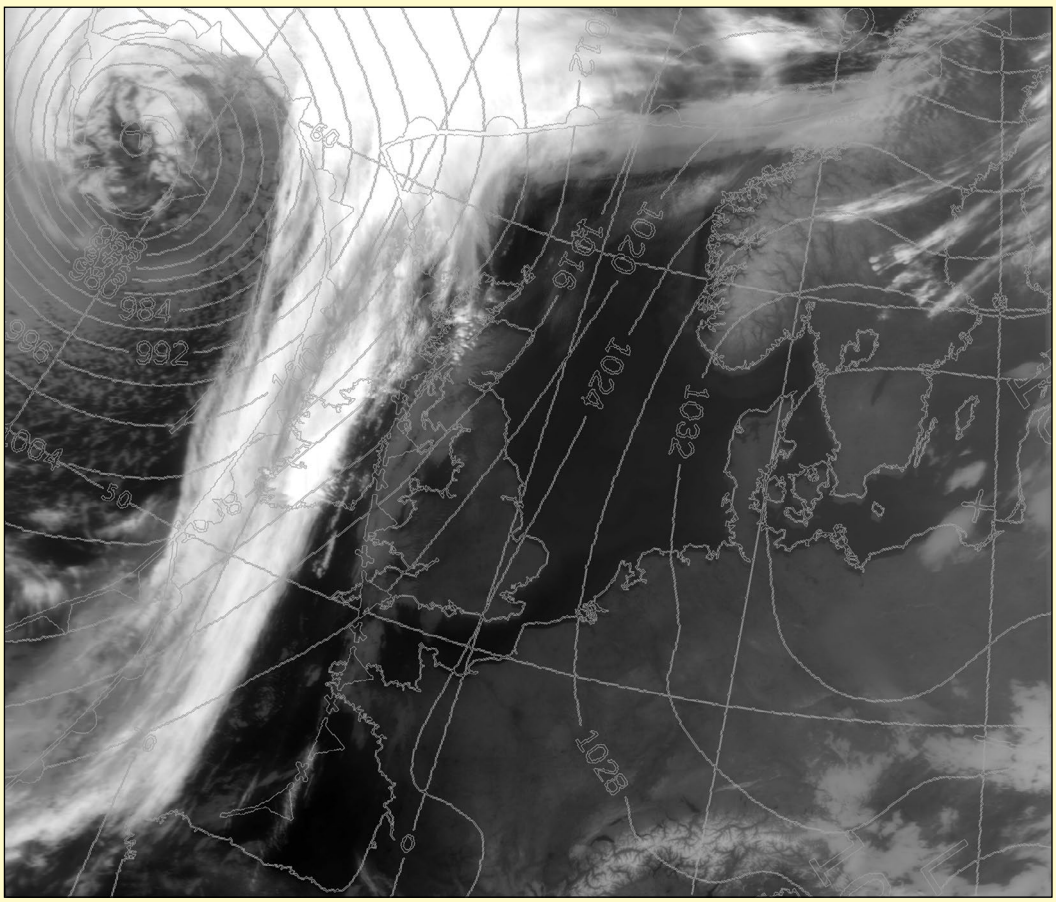

Captured at 17.51 UT on the same day, this infrared image graphically illustrates the deep low pressure system.

Namib Sand Sea

NASA Earth Observatory

Story by Kathryn Hansen

The Namib Desert in southwestern Africa is considered the oldest desert on Earth. It also gives rise to some of the planet's tallest dunes.

Many of the highest dunes are found within the Namib Sand Sea, a section of the desert that spans 34,000 square kilometres of coastal Namibia. The sand sea and its dunes are visible in figure 1, acquired on January 20, 2020, with the HawkEye [1,2] sensor on the SeaHawk CubeSat.

Most of the sand originated from erosion processes that occur to the south of this scene, near the Orange River valley. The Orange River carries sandy sediment into the Atlantic Ocean, and then northward flowing currents move it along the coast and deposit it along the shore. Strong prevailing winds out of the south also can pick up sand and deliver it to the Sand Sea.

Sculpted by winds, the dunes are visible throughout the Sand Sea. Crescent dunes (barchans) appear closest to the shore and are shaped by onshore winds. Farther inland, linear dunes dominate, interrupted in places by patches of star dunes shaped by wind blowing from all directions. Dune 45, visible in figure 2 and the photograph on page 15, is an example of a star dune. Composed of 5-million-year-old sands, Dune 45 towers 80 metres over the desert floor on the eastern flank of the Sand Sea.

Other large dunes—including the Sand Sea's tallest, a 325-meter dune nicknamed 'Big Daddy'—line the bed of the Tsauchab River. The Tsauchab originates in the Naukluft Mountains, then cuts across the Sand Sea before coming to an end at Sossusvlei, a salt and clay pan about 40 kilometres from the Sand Sea's

Figure 1 - The Namib Desert imaged by SeaHawk on January 20, 2020.

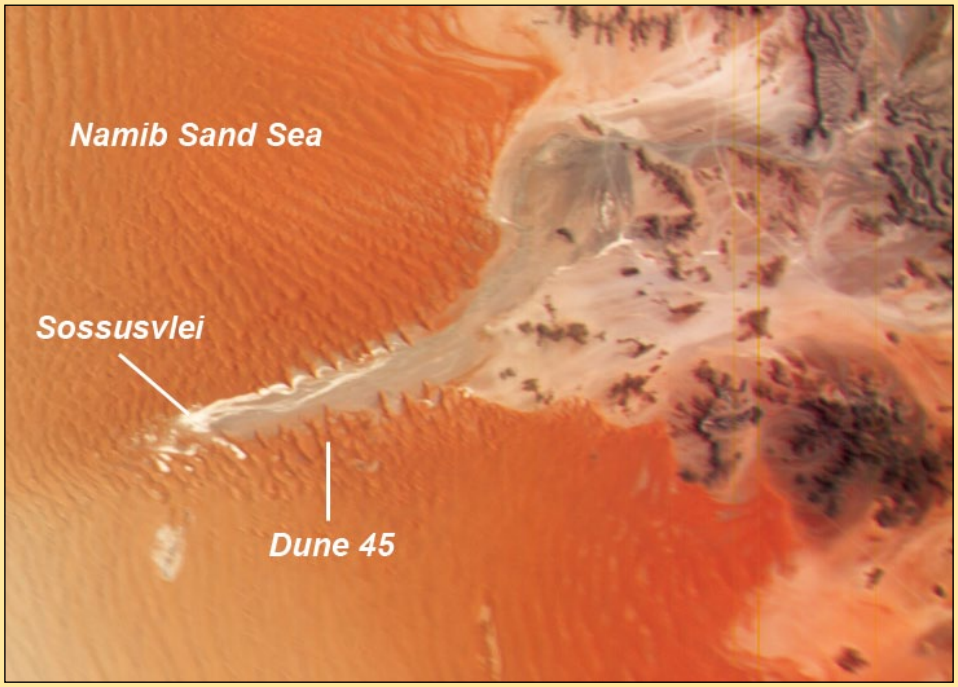

Figure 2 - A zoom into the detailed panel above, highlighting Dune 45

NASA image by Alan Holmes/NASA's Ocean Color Web, using data from SeaHawk/HawkEye.

Figure 3 - Dune 45
Photo courtesy of pxfuel - https://www.pxfuel.com/

eastern flank. Like most rivers and streams in the region, the Tsauchab is ephemeral. Water tends to flow in the Tsauchab and pool up in Sossusvlei every few years or so, generally after a rare heavy rainstorm. In the 2020 view above, the riverbed and clay pans are dry. White areas are probably salt.

Still, life has found a unique way to survive, even without much rain. Fog is the primary source of water for the Namib Sand Sea, which is the only coastal desert in the world to contain large dune fields influenced by fog. This moisture results in relatively abundant and diverse vegetation, particularly on the rocky hills or mountains (inselbergs) that rise above the desert.

References

1 Seahawk/Hawkeye
https://oceancolor.gsfc.nasa.gov/data/hawkeye/
2 The Seahawk 3U Cubesat
https://uncw.edu/socon/seahawk.html

Tenerife, Canary Islands

European Space Agency

Located in the Atlantic Ocean, opposite the northwest coast of Africa, the Canary Islands consist of eight main islands including Gran Canaria, Lanzarote and La Palma, as well as Tenerife and many small islands and islets.

Teide National Park, located in the centre of the island, is a UNESCO World Heritage Site and includes Mount Teide which dominates Tenerife. Rising to around 3718 metres above sea level, its summit is the highest point on Spanish soil. However, much of the volcano's height is hidden. If measured from the ocean floor, its height of 7500 m makes Teide the third-highest volcano in the world.

Teide is an active volcano: its most recent eruption occurred in 1909 when a lava flow buried much of the town and harbour of Garachico on the northern coast.

Owing to the island's diverse topography and unique climatic factors, Tenerife has multiple microclimates, which means that the weather can vary drastically from one part of the island to another. Weather and climate are heavily influenced by the trade winds blowing from the northeast for most of the year, bringing humidity and precipitation to the north of the island, as well as to the northern slopes of Mount Teide. This effect can be clearly seen in the dark green colours in the image, which show vegetation cover. This band of green generally follows the boundary of *Corona Forestal Natural Park*, which covers a total area of 46 000 hectares.

Most of Tenerife's inhabitants live on the lower slopes, within a few kilometres of the sea. Around half the population lives is in or near the cosmopolitan capital of Santa Cruz de Tenerife, located on the southern coast of the narrower northeast part of the island, and San Cristóbal de la Laguna, the former capital. Other

The island of Tenerife, imaged by Sentinel-2
Contains modified Copernicus Sentinel (2021), processed by ESA, CC BY-SA 3.0 IGO

Mount Teide in Tenerife
Photo: James Dawn / Creative Commons Attribution-Share Alike license 3.0

inhabitants live on the intensively cultivated slopes near the northern coast, where the chief towns are La Orotava, Los Realejos, and Puerto de la Cruz. The south of Tenerife is a popular destination where holidaymakers enjoy time on the beautiful beaches of Costa Adeje.

Tenerife is home to Teide Observatory, located around 10 kilometres from Santa Cruz de Tenerife on the Izaña mountain, which is home to ESA's IZN-1 laser ranging station – the first laser ranging station to be made commercially available. It is from here that lasers are aimed into Earth's skies, seeking out satellites—and soon pieces of space junk—as well as measuring their positions and trajectories to prevent catastrophic collisions.

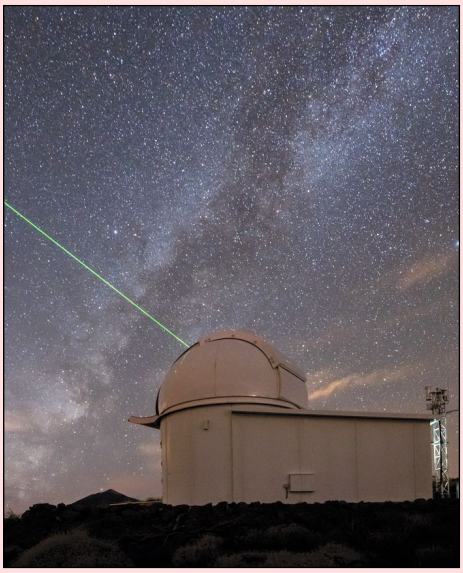

ESA's IZN-1 laser ranging station
Photo: ESA

ESA's IZN-1 laser ranging station on top of the Izaña mountain in Tenerife, Spain, has recently undergone months of testing and commissioning, passing its final tests with flying colours. As it reached 'station acceptance', it was handed over to ESA by DiGOS, the German company contracted to build it. The station is a technology test-bed and a vital first step in making debris mitigation widely accessible to all space sectors with a say in the future of our space environment.

Read more about ESA's laser ranging station at

https://www.esa.int/Safety_Security/Space_Debris/New_laser_station_lights_the_way_to_debris_reduction

Santa Cruz de Tenerife, capital city of the island.
Image ESA

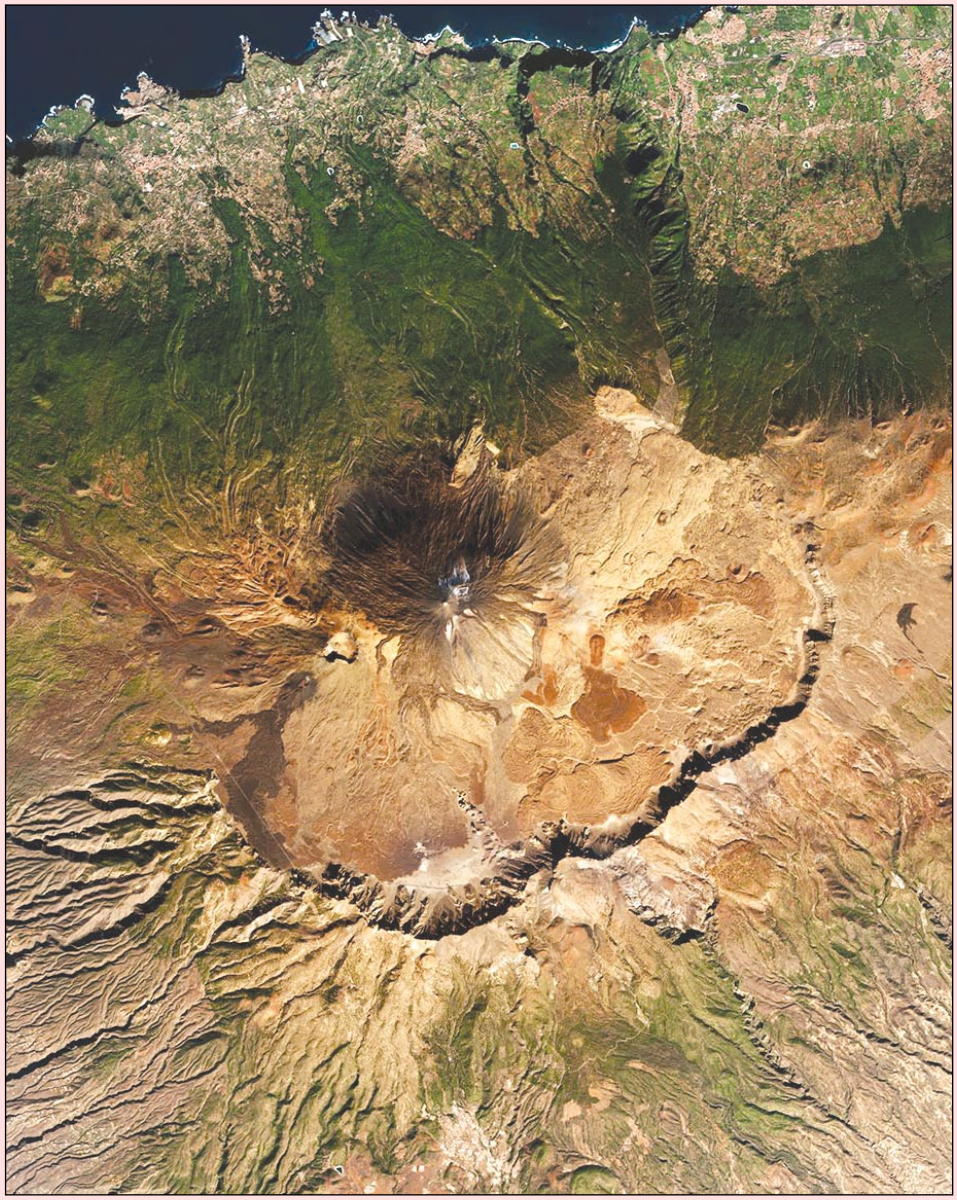

Mount Teide National Park on Tenerife. The volcano is in the centre of this scene.
Image ESA

LANDSAT: The Satellite That Might Save the Earth

Part 2 – The Imagers and Applications

Ed Murashie

Only Landsat images can show how Las Vegas, Nevada, USA has rapidly expanded over the past 50 years when viewed from space. This is because Landsat is the longest running Earth resources satellite program and has been in continuous operation since 1972. That's probably why the USGS, the folks that run the Landsat program, chose 'Science for a changing world' as their slogan. But with technology advancing as fast as it has, how is comparing decades of imagery even possible? This should be like comparing a picture taken by a 1972 Kodak Instamatic film camera with another taken by a modern cellphone camera. The answer is, lots of planning and an understanding of the imager's evolution.

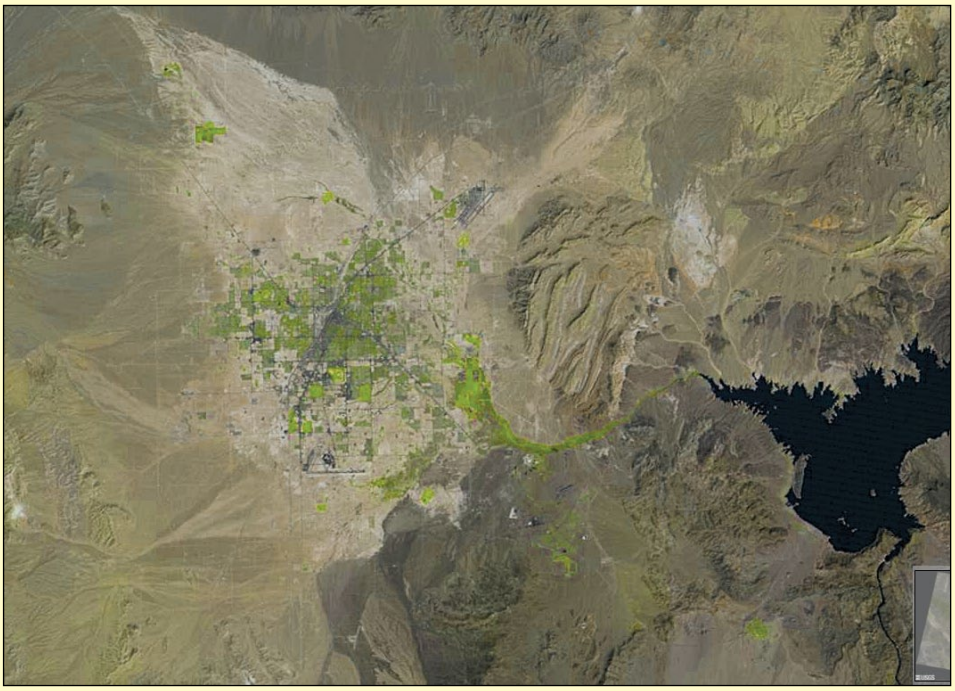

Las Vegas as seen by Landsat-1 on Sept 13, 1972
Image courtesy of the U.S. Geological Survey

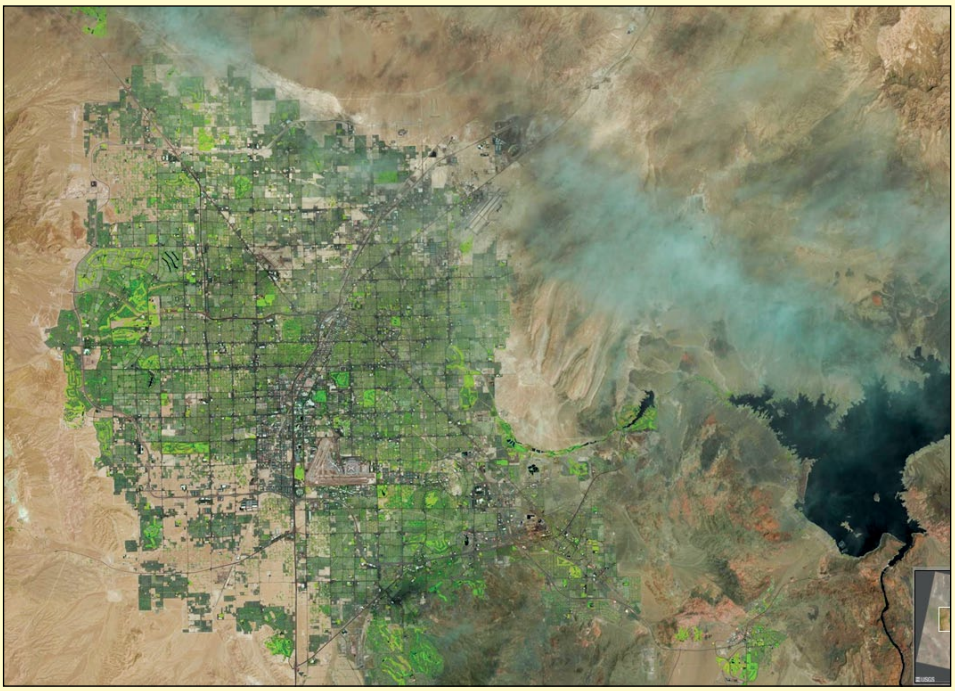

The same scene as Las Vegas was viewed from Landsat-8 on May 15, 2013
Image courtesy of the U.S. Geological Survey

Landsat Imager Evolution

Return Beam Vidicon: Landsat 1-3

Landsat 1, 2, and 3 carried two imagers. The primary imager was the gold standard analog return beam vidicon (RBV) imager similar to the one flown on the TIROS and early Nimbus spacecraft. One RBV limitation was that it was only operated during daylight, but an advantage was that the Earth scene could be imaged instantaneously like a camera. The imagers' characteristics are shown diagrammatically on page 19 and in detail in Table 1 overleaf.

Multispectral Scanner: Landsat 1-5

The secondary imager was a new experimental digital multispectral scanner (MSS) and was the first digital imager flown on **any** spacecraft. Sunlight reflected from the Earth was in turn reflected by a rotating mirror and focused on a set of filters and detectors with an optical telescope. The angled spinning mirror caused a west-to-east scan of the Earth, while the spacecraft's orbital motion caused a north-to-south scan. This is the same technique used in the NOAA weather satellite's AVHRR imager. Because the west-to-east scanning is like a broom sweeping from side-to-side, this type of imager is referred to as a 'whiskbroom' imager. There are two interesting MSS facts to make note of. One is that during Landsat 1's 196th orbit, the RBV power relay stuck in its 'on' position and, instead of trying to correct the problem, the imager was left off since the MSS proved to be the superior imager. The other fact is that Landsat 1-3's orbital altitude was approximately 900 km, while that of Landsats 4 and 5 were at 700 km. And, because the program wanted satellite data compatibility, they redesigned Landsat 4 and 5's MSS optics to maintain the 79 m resolution. As an experiment, Landsat 3's RBV was redesigned to just have one channel with higher resolution than its MSS imager.

contiued on page 20

Imager	Spacecraft	Swath Width	Channel	Wavelength (um)	Resolution (m)	Fidelity	Notes
RBV	Landsat 1-2	183 km	1	0.48-0.57	80	Analog	
			2	0.58-0.68	80	Analog	
			3	0.70-0.83	80	Analog	
	Landsat 3	183 km	1	0.505-0.75	40	Analog	
MSS	Landsat 1-5	185 km	1	0.5-0.6	79	6 bits Digital	Green
			2	0.6-0.7	79	6 bits Digital	Red
			3	0.7-0.8	79	6 bits Digital	Near infrared
			4	0.8-1.1	79	6 bits Digital	Near infrared
TM	Landsat 4-5	185 km	1	0.45-0.52	30	8 bits Digital	Blue
			2	0.52-0.60	30	8 bits Digital	Green
			3	0.63-0.69	30	8 bits Digital	Red
			4	0.76-0.90	30	8 bits Digital	Near infrared
			5	1.55-1.75	30	8 bits Digital	Short wave infrared
			6	10.4-12.5	120	8 bits Digital	Thermal infrared
			7	2.08-2.35	30	8 bits Digital	Short wave infrared
ETM+	Landsat 7	183 km	1	0.45-0.52	30	9 bits Digital	Blue
			2	0.52-0.60	30	9 bits Digital	Green
			3	0.63-0.69	30	9 bits Digital	Red
			4	0.77-0.90	30	9 bits Digital	Near infrared
			5	1.55-1.75	30	9 bits Digital	Short wave infrared
			6	10.40-12.50	60	9 bits Digital	Therma infrared
			7	2.09-2.35	30	9 bits Digital	Short wave infrared
			8	0.52-0.90	15	9 bits Digital	Panchromatic
						2 gain states 8 bits transmitted	
OLI/OLI-2	Landsat 8-9	185 km	1	0.433-0.453	30	12 bits Digital	Deep blue
			2	0.45-0.515	30	12 bits Digital	Blue
			3	0.525-0.60	30	12 bits Digital	Green
			4	0.63-0.68	30	12 bits Digital	Red
			5	0.845-0.885	30	12 bits Digital	Near infrared
			6	1.56-1.66	30	12 bits Digital	Short wave infrared
			7	2.1-2.3	30	12 bits Digital	Short wave infrared
			8	0.50-0.68	15	12 bits Digital	Panchromatic
			9	1.36-1.39	30	12 bits Digital	Short wave infrared
TIRS/TIRS-2	Landsat 8-9	185 km	1	10.3-11.3	100	12 bits Digital	Thermal infrared
			2	11.5-12.5	100	12 bits Digital	Thermal infrared

Table 1 - Landsat Imager Characteristics

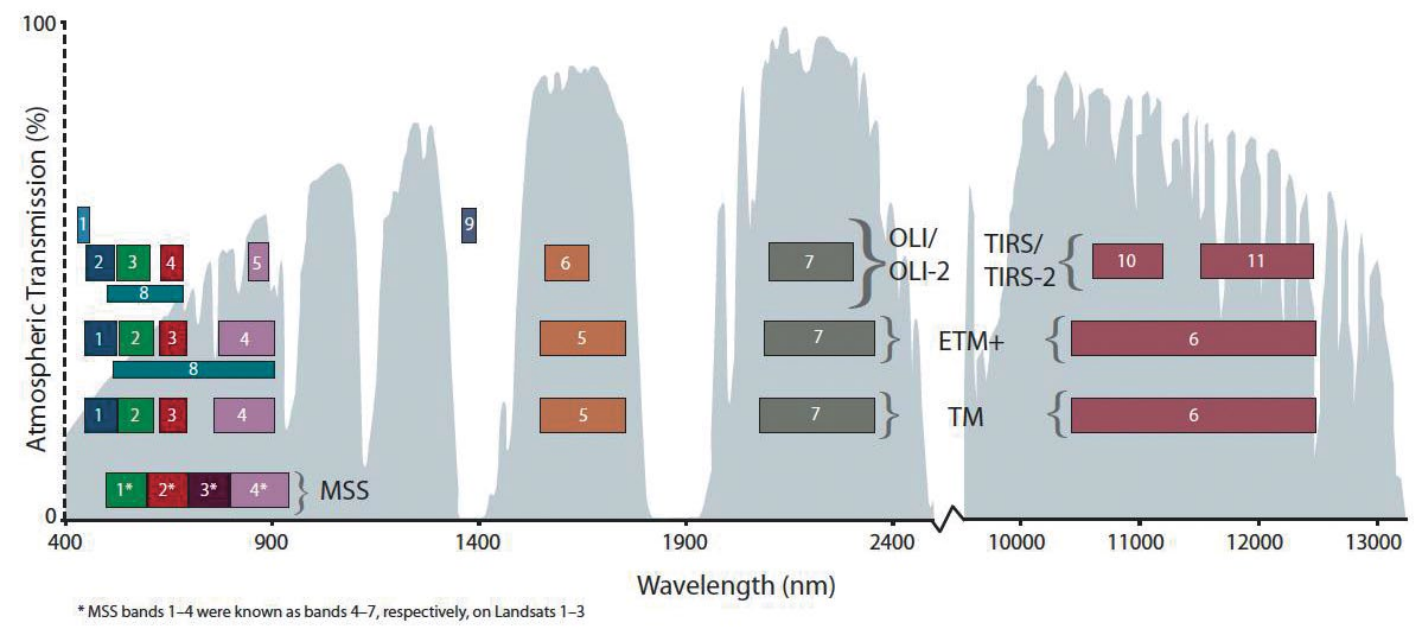

Figure 1: Landsat 1-9 Digital Imager Band Chart. (Chart courtesy of the U.S. Geological Survey)

Thematic Mapper: Landsat 4-5

Santa Barbara Research Center, the designers of the MSS, designed the follow-on improved Thematic Mapper (TM) imager used on the Landsat 4 and 5 satellites. The TM 'whiskbroom' imager improved the spatial resolution from 79 m to 30 m, tightened the spectral resolutions, improved the radiometric resolution from 6 bits to 8 bits, and added three new bands. Radiometric resolution relates to the number of gray shades an imager can discern. Increasing from 6 bits to 8 bits means going from 64 shades of gray to 256. The added bands were blue, short wave infrared and thermal infrared. The added blue band allowed red, green and blue images to be combined to make natural color images.

The short wave infrared image can help in identifying certain minerals, measure plant health and see through smoke or haze. Thermal infrared sensors measure the heat given off by objects unlike the other sensors which measure reflected light. They are suited for measuring sea surface temperatures, fire detection and other thermal mapping applications. You may notice different applications, or themes, were mentioned in describing the new bands. This is where the thematic mapper got its name. Scientists were now using existing and added bands to create application maps for different Earth science studies. The TM also changed from a unidirectional scanning sweep to a bi-directional scanning sweep, and added a sweep corrector to eliminate the satellite orbital motion component in images. More about the sweep corrector later.

Enhanced Thematic Mapper and Enhanced Thematic Mapper Plus: Landsat 6-7

Only Landsat 6 carried the new Enhanced Thematic Mapper (ETM) but since Landsat 6 failed to reach orbit, the ETM was never operated.

Raytheon bought *Hughes* and renamed *Santa Barbara Research Center*, *Santa Barbara Remote Sensing*. *Santa Barbara Remote Sensing* designed the Enhanced Thematic Mapper Plus (ETM+) which was the only imager aboard Landsat 7. The ETM+ is also a 'whiskbroom' type imager with a sweep corrector. Unfortunately the sweep corrector failed in May 2003, so there have been image gaps at the ends of image scenes since. The ETM+ added a 15 m resolution panchromatic band and increased the radiometric resolution from 8bits to 9 bits. It has a dual gain selector which determines and then transmits the best range of 8 bits. The panchromatic band, with its higher resolution, allows image sharpening when applied to the other bands. Another major ETM+ feature is improved calibration and radiometric accuracy.

Operational Land Imager and Operational Land Imager-2: Landsat 8-9

Landsat 8 and 9 carry two new imagers each: the Operational Land Imager (OLI) and the Thermal Infrared Sensor (TIRS) on Landsat 8, and the OLI-2 and TIRS-2 on Landsat 9. The OLI was built by *Ball Aerospace and Technologies Corporation*. Unlike the 'whiskbroom' design, both the OLI and TIRS are 'pushbroom' designs, meaning there is a full west-to-east scan line of detectors, with the satellite' orbital motion providing the north-to-south scanning. 'Pushbroom' designs have proven themselves on other types of satellites, with advantages including instantaneous full image capture, no moving parts, and lighter weight. Disadvantages include the increased calibration complexity of the 69,160 detectors and far more detectors than previous designs. The previous designs would run a simpler calibration routine at the ends of each scan line.

Other OLI improvements over the ETM+ include two new channels and a radiometric resolution increase from 8 bits equal to 256 shades of gray to 12 bits equal to 4096 shades of gray. The added channels are 'deep blue' for studying aerosols and the coastal zones, and a short wave-Infrared which is optimized for cirrus cloud detection. The OLI-2 designs are similar to the OLI, with a few improvements such as having 14 bits of radiometric resolution so that darker scenes can be better imaged.

Thermal Infrared Sensor and Thermal Infrared Sensor-2: Landsat 8-9

Landsat 8 and 9 carry dedicated twin channel 'pushbroom' thermal scanners, TIRS and TIRS-2, both built by NASA's *Goddard Spaceflight Center*. Two TIRS-2 improvements include reducing stray light and added redundancy.

By having a consistent set of base bands, adding new bands, improving accuracy, increasing spatial and radiometric resolution, Landsat has been able to allow nearly 50 years of data comparisons while taking advantage of new technologies.

Landsat Data Applications

With a unique complement of sensor bands, a long retrospective and global view of Earth, there are a wide range of applications that rely on Landsat's data. Applications include mapping, agricultural, mineral exploration, disaster monitoring, and studying land and water use. People who use the data include government agencies, educational institutions, private companies and even farmers. One agency that supports others with Landsat education, applied research, workforce development, technology transfer and community outreach is *AmericaView*. To learn more go to their website at

https://americaview.org/

Interesting Landsat data applications

Evapotranspiration

Water follows a cycle. A simplistic view of the water cycle is rain falling to the Earth, being heated by the sun, and evaporating back into the atmosphere to start the cycle again. But water can also be absorbed by vegetation and the leaves give back the moisture to the atmosphere through transpiration. When combining evaporation and transpiration, the term evapotranspiration is formed. When transpiration occurs, it cools off the soil and vegetation. Landsat sensors can measure the temperature using the TIRS, and when combined with other environmental data such as wind, an evapotranspiration (ET) number can be calculated.

Knowing how much moisture is leaving a crop can give farmers an idea of how much water must be applied to keep a healthy balance. *OpenET.org* is one organization that makes the ET data available on their website

https://openetdata.org/

where you can display a map, zoom in to individual farm plots using the 30 meter resolution Landsat data, and display the ET data over time (figure 2).

LANDFIRE

As you probably have seen in the news, California is subject to major wildfires, and the state and federal government have spent millions on wildfire operations. Part of those operations including planning. LANDFIRE is a joint program between the U.S. Department of Agriculture Forest Service and U.S. Department of the Interior.

Its LANDFIRE Data Distribution Site map relies on Landsat and other data to provide landscape geo-spatial data (figure 3) to support wildfire planning, management, and operations. The tool allows you to map data sets ranging from brush coverage to vegetation types all at the click of the mouse. To learn more go to

https://landfire.gov/about.php

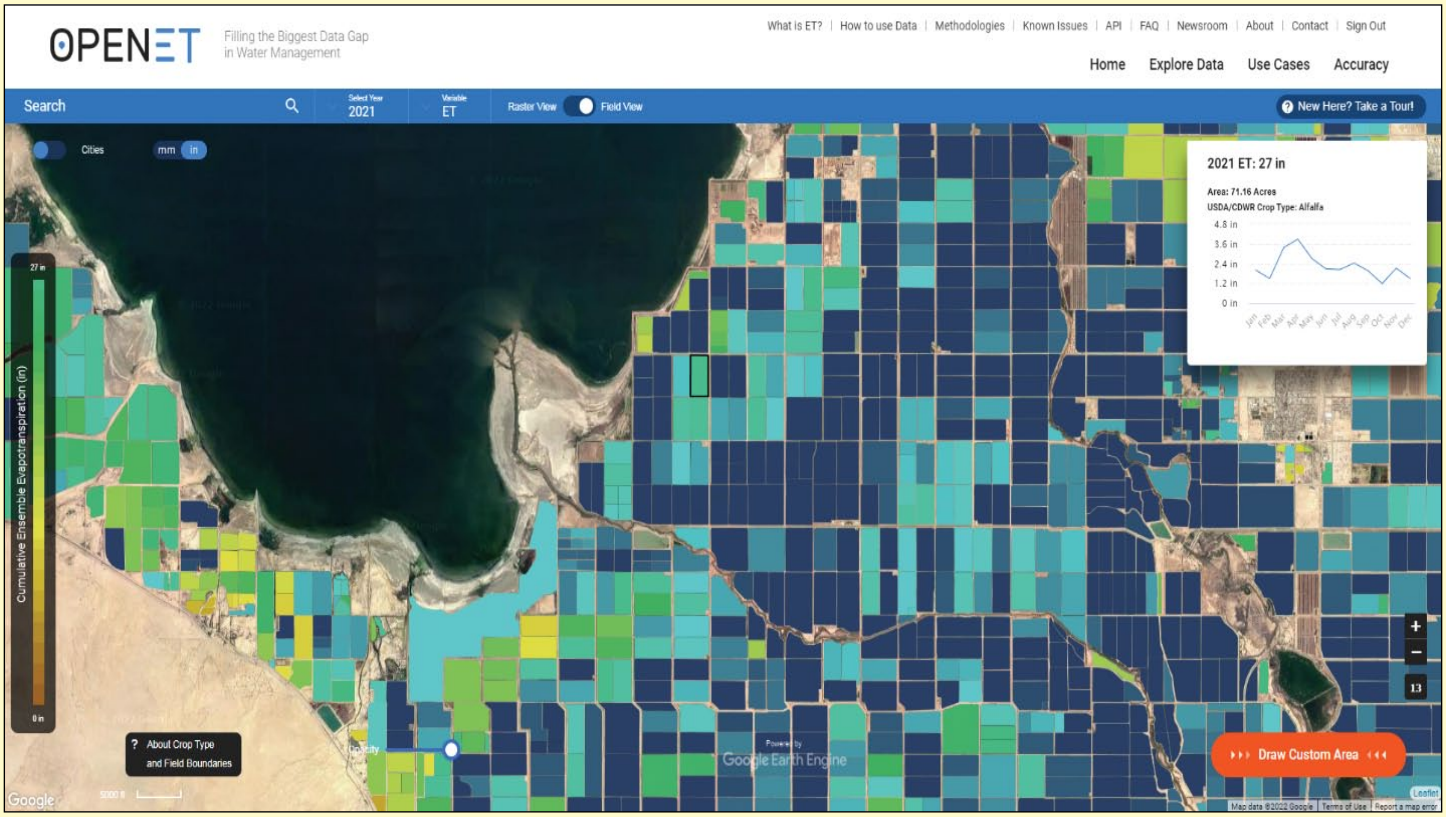

Figure 2 - Evapotranspiration
Image courtesy of OpenET.

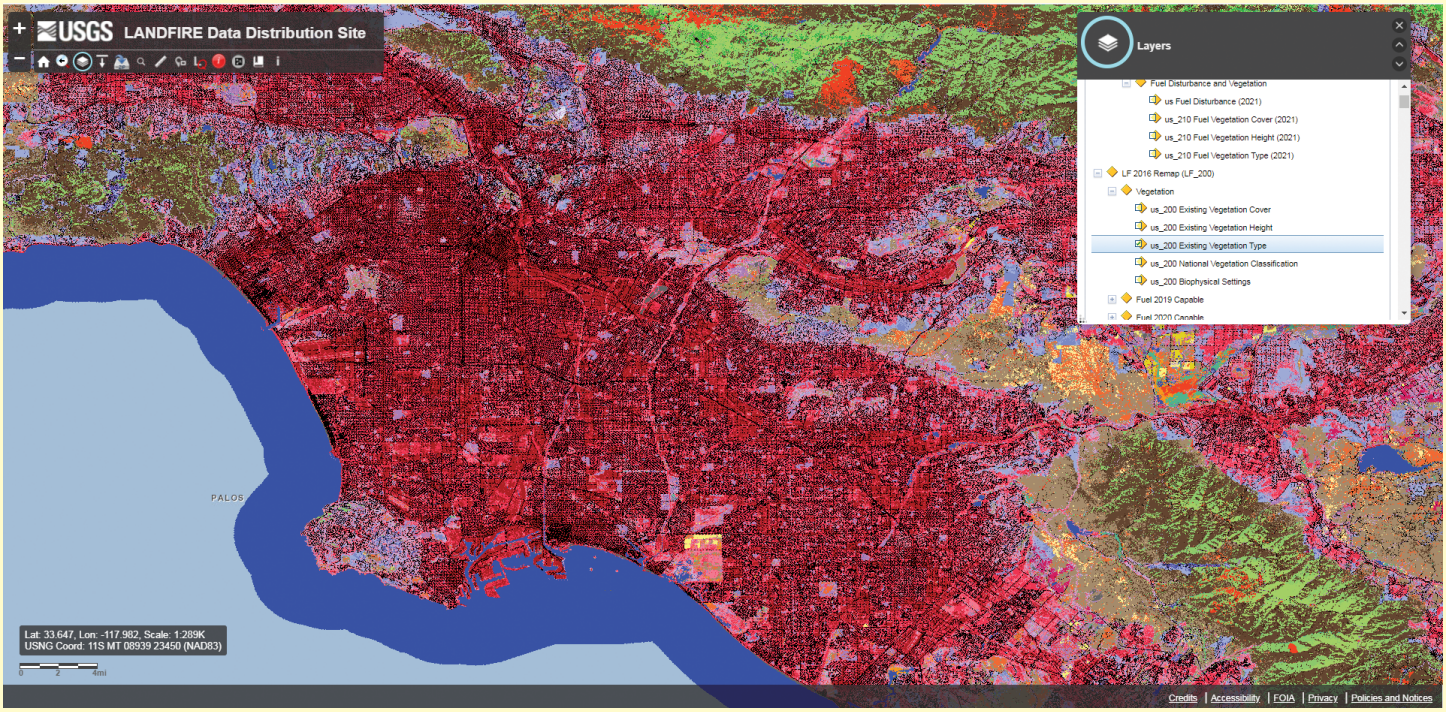

Figure 3 - Los Angeles California Map
Image courtesy LANDFIRE.

Figure 4 - Landsat and the Calypso Caper YouTube Banner
Image courtesy NASA

Jacques Cousteau

What does one of the world's most famous oceanographers, an Apollo 9 astronaut, and Landsat have in common? They all worked together during the summer of 1975 to prove if satellite bathymetry was possible, and it turns out that it is.

Satellite bathymetry is the science of measuring shallow ocean water depth using satellite data, in this case it used Landsat 1 and Landsat 2 bands 4 and 5 MSS data. It is an important measurement, since it is estimated that 80% of all goods are carried by ships, and shallow waters pose a hazard. A team of divers, Jacques Cousteau, Astronaut Rusty Schwikart, the president's son Jack Ford and others gathered on the Calypso and set sail for Montego Bay. With its clear shallow waters it made for a perfect place to practice.

From there they sailed to the Bahamas, met up with a sailboat and started making their measurements. The Calypso's radar took depth measurements and, as Landsat came overhead, divers made temperature, horizontal and vertical visibility measurements, sea floor images and samples. Every night the boats would sail to a new location

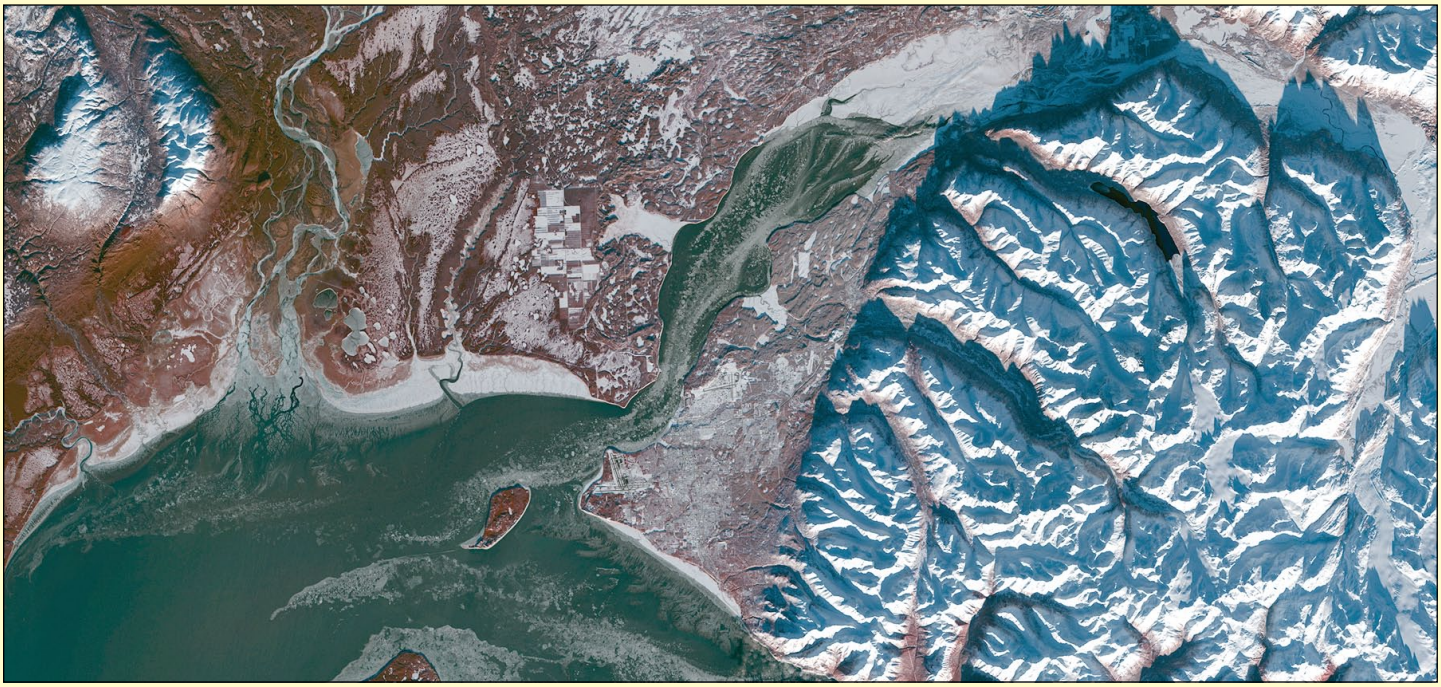

Figure 5 - This false color image of the Anchorage area, Alaska, was observed by the recently launched Landsat-9 on November 20, 2021. The image was built using infrared, red, and blue bands of the electromagnetic spectrum and illustrates the satellite's resolving power.
Image: NASA / USGS

in a grid pattern to make the same measurements. The principal is to measure the sun energy as it passes through the air, water and reflected off the ocean bottom.

A mathematical model was created using the MSS green band 4 and red band 5 high gain data plus the viewing and refracted sun angle. Analyzing the data showed that satellite bathymetry was possible up to 22 meters depth and helped revise waterway charts.

I have just touched upon a few applications but there are countless more. One resource that explores 120 applications can be found at

https://grindgis.com/blog/120-landsat-data-applications

while at NASA's Goddard Spaceflight Center's webpage

https://landsat.gsfc.nasa.gov

you can learn more about the satellite and its uses.

Learn more about the '*Landsat and the Calypso Caper*' on YouTube at

https://www.youtube.com/watch?v=3pSctnQy3B4

Conclusion

In Part 3 you will learn where to download the images, and how to use free tools to manipulate the images.

You will be able to apply what you have just learned about the imagers and data applications to explore the Earth on your own.

Russia's Crater of Diamonds

Continued from page 10

thick and about 12 to 13 km away from the impact site. Scientists estimate that diamonds did not form at the impact site because the collision's heat and pressure were likely too great to survive there.

Popigai crater is the site of one of the largest diamond fields in the world today, estimated to contain 'trillions of carats.' Because they were formed instantly, the 'impact diamonds' did not have time to develop as large, single gemstones. Most are polycrystalline stones smaller than two millimeters and with low purity, making them better for industrial uses than for jewellery.

A new eruption started at the Anak Krakatoa, or Krakatau, volcano on Rakata Island in Indonesia on February 3 2022, as shown in this image captured by the Copernicus Sentinel-2 mission. The eruption started at around 16:15 local time, with a thick column of gas, with possible volcanic ash content, rising to around 200 metres above the crater.

Image contains modified Copernicus Sentinel data (2022), processed by ESA, CC BY-SA 3.0 IGO

Tidal Vortices in the Sea of Okhotsk

NASA Earth Observatory

Story by Sara E. Pratt

NASA image by Norman Kuring/NASA's Ocean Color Web,
using Landsat data from the U.S. Geological Survey.

Some of the highest diurnal tides in the world—nearly 14 metres—have been recorded in the Sea of Okhotsk. In the Russian Far East, narrow bays funnel and amplify the incoming tides, making it a prime location for tidal power generation.

The transition from smooth, laminar flow to mixed, turbulent flow is visible in this natural-colour image of tidal currents in the western Sea of Okhotsk. The image of the Shantar Islands and Uda Bay was acquired on September 24, 2021, by the Operational Land Imager (OLI) on Landsat 8.

The currents around the Shantar Islands are heavily influenced by the strong tides and by freshwater discharge from rivers draining into Uda Bay. The waters here are frozen for much of the year. When the sea ice melts and freshwater snowmelt swells the Uda River, plumes of low-salinity water can reach far offshore.

As the strong tides and currents flow through straits in the Shantar Islands, they encounter rocky outcrops, headlands, capes, and small islands that disrupt the laminar flow. This can create chains of spiral eddies that rotate in alternate directions as they form. These chains are known as vortex streets or von Kármán vortices. The physical processes that create the vortices were first described in 1912 by Theodore von Kármán, a Hungarian-American physicist and a co-founder of NASA's Jet Propulsion Laboratory. In the Shantar Islands, vortices in the chain propagate mainly to the east at low tide and to the west at high tide.

After abundant snowfall on 8 December 2021, here's a rare cloud-free Copernicus Sentinel-2 mission mosaic image of Liguria, Valle D'Aosta, Piedmont, Lombardy and a little portion of Tuscany in Italy. Monte Rosa can be seen at the top left corner of the image.

Image contains modified Copernicus Sentinel data (2021), processed by ESA, CC BY-SA 3.0 IGO

Lake Manicouagan

MODIS Web Image of the Day

Lake Manicouagan

Once nominated as one of the '*Seven Wonders of Canada*', the curiously circular Lake Manicouagan draws attention both from land-bound tourists and from space. Tourists and fishermen adore the lake for spectacular scenery and excellent salmon fishing. And the striking appearance of the 'eye of Quebec' allows rapid orientation to astronauts and satellites, confirming that there is no other place on Earth quite like this striking structure. In fact, it was an astronaut, Marc Garneau, who nominated this reservoir for the Seven Wonders of Canada competition.

Lake Manicouagan spans an area of 1,942 sqare kilometres in central Quebec, Canada and has a volume of 139.8 cubic kilometres, making the reservoir the fifth largest in the world by volume. The large island in the center of the lake is called René-Levasseur Island and helps give the lake it's eye-like appearance.

The lake's peculiar appearance comes from its creation. Lake Manicouagan sits in an ancient and heavily eroded impact crater (astrobleme) from an asteroid which struck the Earth about 214 million years ago. The original diameter of the impact has been estimated to have been about 100 kilometres, and the size of the asteroid at about 5 kilometres in diameter. Glaciation and other erosional processes have reduced the extent of the crater, leaving its visible diameter at only 72 kilometres, still the sixth-largest confirmed impact crater on Earth.

The Moderate Resolution Imaging Spectroradiometer (MODIS) on board NASA's Aqua satellite acquired this stunning true-colour image of frozen Lake Manicouagan on January 11, 2022. Frigid weather has frozen Lake Manicouagan as well as other lakes and rivers in the region, while light snowfall sits on the surrounding landscape.

Ukraine Under Attack

Thanks to Ed Murashie for forwarding this revealing image acquired by the USGS Landsat-8 satellite.

Captured by the satellite's Night Acquisition Band, the image details the streets of the city of Kryvii Rih (located about 300 kilometres southeast of the capital city Kyiv) and shows hotspots of enemy activity as bright highlights in its southeast quarter. Kryvii Rih is the largest city in central Ukraine and the seventh most populous in the country with around three-quarters of a million inhabitants.

Image: USGS

Seeing Suomi

NASA Earth Observatory

Story by Michael Carlowicz

It is the land of reindeer husbandry—one of the few places on Earth where these deer have been domesticated. It is the home of Europe's only recognised indigenous people. It is also the ancestral homeland of 'The Father of Satellite Meteorology.' Welcome to Scandinavia.

The image above is part of a global composite assembled from data acquired in 2016 by the NOAA-NASA Suomi National Polar-orbiting Partnership (Suomi NPP) satellite. This night time view of Scandinavia was made possible by the 'day-night band' of the satellite's *Visible Infrared Imaging Radiometer Suite*. VIIRS was built to be sensitive enough to measure night time light emissions and reflections, to distinguish the intensity of lights and to observe how they change.

The satellite was named after Verner Suomi, a meteorology researcher and revered longtime professor at the University of Wisconsin–Madison.

https://earthobservatory.nasa.gov/features/Suomi

Suomi built a flat-plate radiometer that was launched on the Explorer 7 satellite in October 1959. It was the first of several Earth-observing instruments that Suomi conceived or built over a five-decade career, and he was instrumental in advancing the study of clouds, weather and the planet's radiation budget.

> "*When I first began my work with meteorological satellites, no one in the Department of Meteorology seemed particularly interested*," he was once quoted as saying. "*But they didn't try to impede progress in the field, for which I'm forever thankful.*"

Though he grew up in Minnesota, Suomi was the son of Finnish immigrants from the Aland Islands. In the Finnish language, Suomi is the name for Finland.

The winter scene on the following page comes from the Sápmi region of Finland (formerly known as Lapland), not far from Oulanka National Park. The natural-colour image was acquired on January 30, 2014, by the Operational Land Imager (OLI) on *Landsat 8*. At the time, the Sun was just a few degrees above the southeastern horizon, leading to long shadows in the valleys and golden rays

https://earthobservatory.nasa.gov/images/149235/seeing-suomi

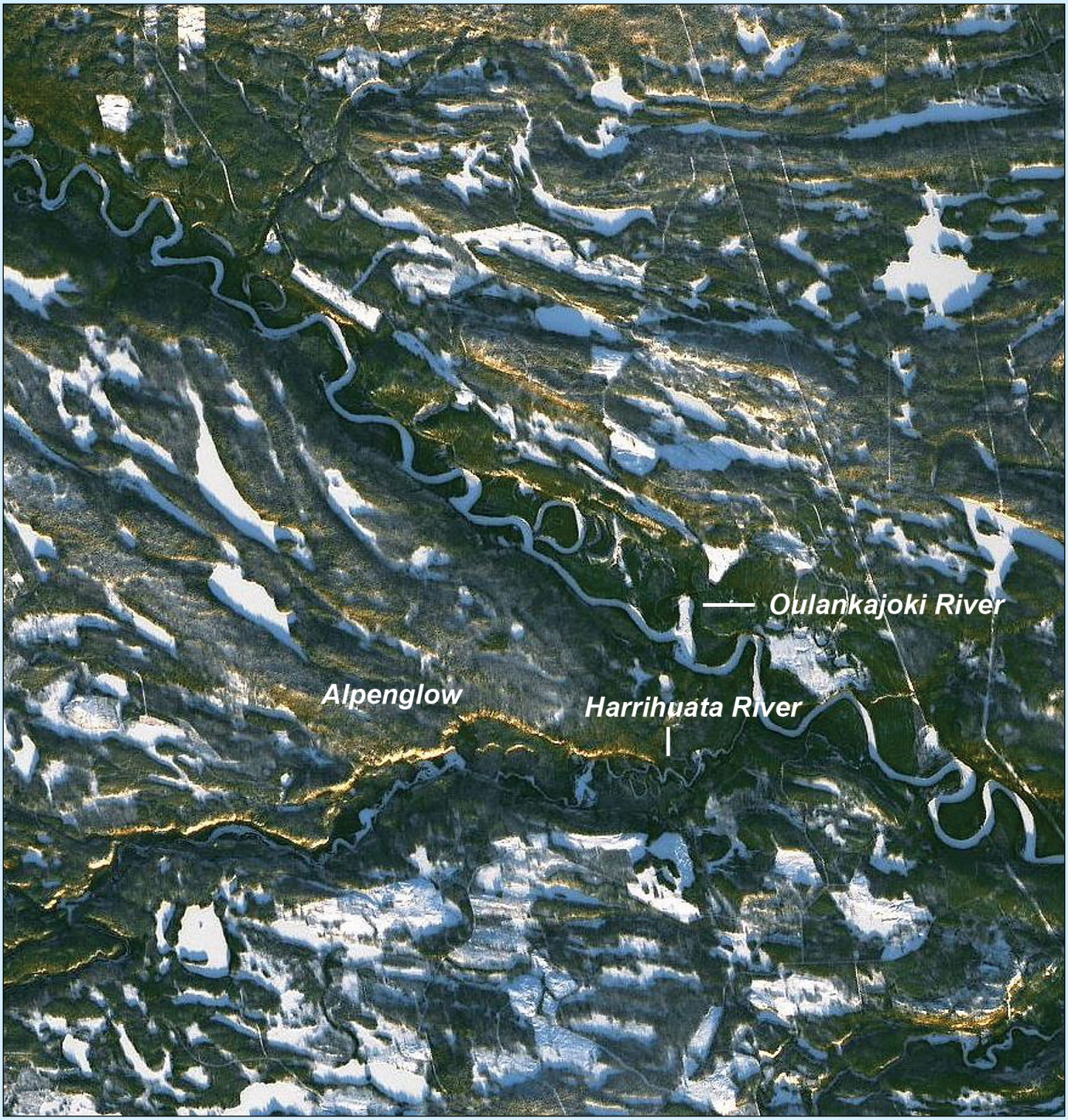

touching the peaks of mountains. Some of the landscape was probably illuminated by alpenglow, a phenomenon where airborne snow, water, and ice reflect sunlight down toward Earth—even if the Sun is below the local horizon.

The Sápmi region stretches across parts of Finland, Sweden, Norway, and Russia, and it is the ancient home of the indigenous Sami people. About 80,000 to 100,000 Sami are spread across the four nations and they have long lived a nomadic life of hunting and gathering, and reindeer herding. An estimated 500,000 reindeer live in Scandinavia, with most of them tended and herded by the Sami.

By some historical accounts, the Sami may have been herding reindeer as far back as the ninth century. Though electronic tools and motorised vehicles have become part of the now semi-nomadic herding life, the ancient Sami languages are still key to animal husbandry in the rugged and cold region. Reindeer and the herding units that tend them are central to the culture, providing meals, tools, clothing and a structure to life amid changing times in northern Europe.

NASA Earth Observatory images by Joshua Stevens, using Black Marble data from NASA/GSFC, Blue Marble imagery by Reto Stöckli, and Landsat data from the U.S. Geological Survey.

Colorado Faces Winter Urban Firestorm

NASA Earth Observatory

Text by Sara E. Pratt

The Marshall fire, imaged on December 30, 2021 by NASA's Aqua satellite.

On December 30, 2021, high winds roared out of the west and down the front slope of the Rocky Mountains in Colorado. Northwest of Denver, peak gusts reached 185 kilometres per hour—the equivalent of a category 3 hurricane. Those winds whipped up intense grass and brush fires in south Boulder and blew them east toward the towns of Superior and Louisville, igniting a firestorm. By the time it was over, nearly 1,100 houses had been destroyed or damaged, two people were reported missing, and thousands were displaced.

The Marshall fire is now the most destructive in the state's history. Four of the top five largest wildfires on record in Colorado occurred between 2018 and 2021. Unlike many of the megafires in the American West in recent years—which typically occur in forests and wildlands—the Marshall fire quickly travelled into densely populated neighborhoods and transitioned from a wildfire to an urban conflagration.

Tens of thousands of residents were evacuated as flames were blown down streets and through cul-de-sacs. The fire was carried by what climate scientist and Boulder resident Daniel Swain called 'an ember storm.' Blown by hurricane-force winds, the embers leapt from house to house, burning many from the inside out, while torching trees, igniting commercial buildings, and jumping a highway.

The natural-coloir image above was acquired just a few hours after the fire started on December 30 by the Moderate Resolution Imaging Spectroradiometer (MODIS) on NASA's Aqua satellite. At the time, the smoke plume—which was also visible on radar—stretched about 100 kilometres over Colorado's eastern plains. The fire also generated its own weather: the rising heat created a low-pressure area that drew surface winds toward the fire from all directions.

The next day brought much-needed moisture, as a cold front moved in and dropped more than 25 centimetres of snow—dampening the fire but also complicating the response. As of January 3, 2022, the perimeter of the 6,200-acre fire was fully contained.

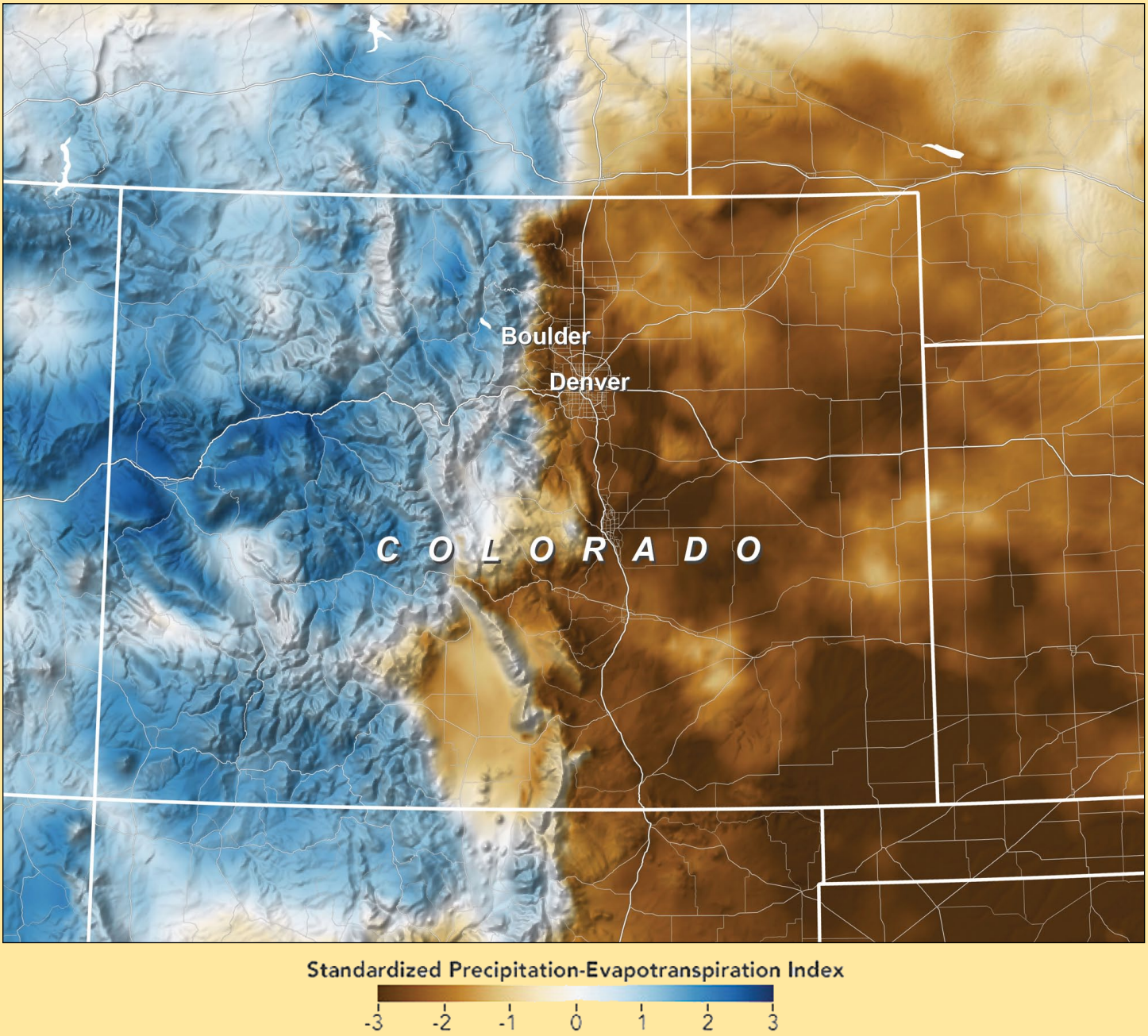

This map shows the *Standardized Precipitation-Evapotranspiration Index* (SPEI) for Colorado for the month of December 2021.

High winds and wildfires are not uncommon on the Front Range, but a December wildfire is, as the normal fire season lasts from May to September. One recent study found that increases in extreme fire weather are being driven by decreases in atmospheric humidity and increasing temperatures.

In 2021, Colorado saw an unseasonably warm summer and fall, coupled with record dryness. The warm, dry spell followed an unusually wet spring, which reduced wildfires through the summer and fueled the growth of vegetation—which then dried out and provided ample tinder for the December fire.

At the time of the fire, the eastern part of Boulder County was classified with extreme drought, according to the U.S. Drought Monitor. The map above shows the *Standardized Precipitation-Evapotranspiration Index* (SPEI) for Colorado for the month of December 2021. It accounts for both precipitation and temperature (it does not include the New Year's snowfall that helped extinguish the fire). According to the *Colorado Climate Center*, SPEI values exceeding minus two are very rare and are indicative of the extreme warm and dry conditions across eastern Colorado.

The map also shows the contrast between the extreme drought in the eastern part of the state, where the fire occurred, and the snowpack in the western part of the state, where significant December snowfalls brought the snowpack near or above average. Denver, which normally has 50 centimetres of snow by late December, did not record its first winter snowfall until December 10, the latest on record.

NASA Earth Observatory images by Joshua Stevens, using MODIS data from NASA EOSDIS LANCE and GIBS/Worldview, and PRISM data courtesy of the West Wide Drought Tracker.

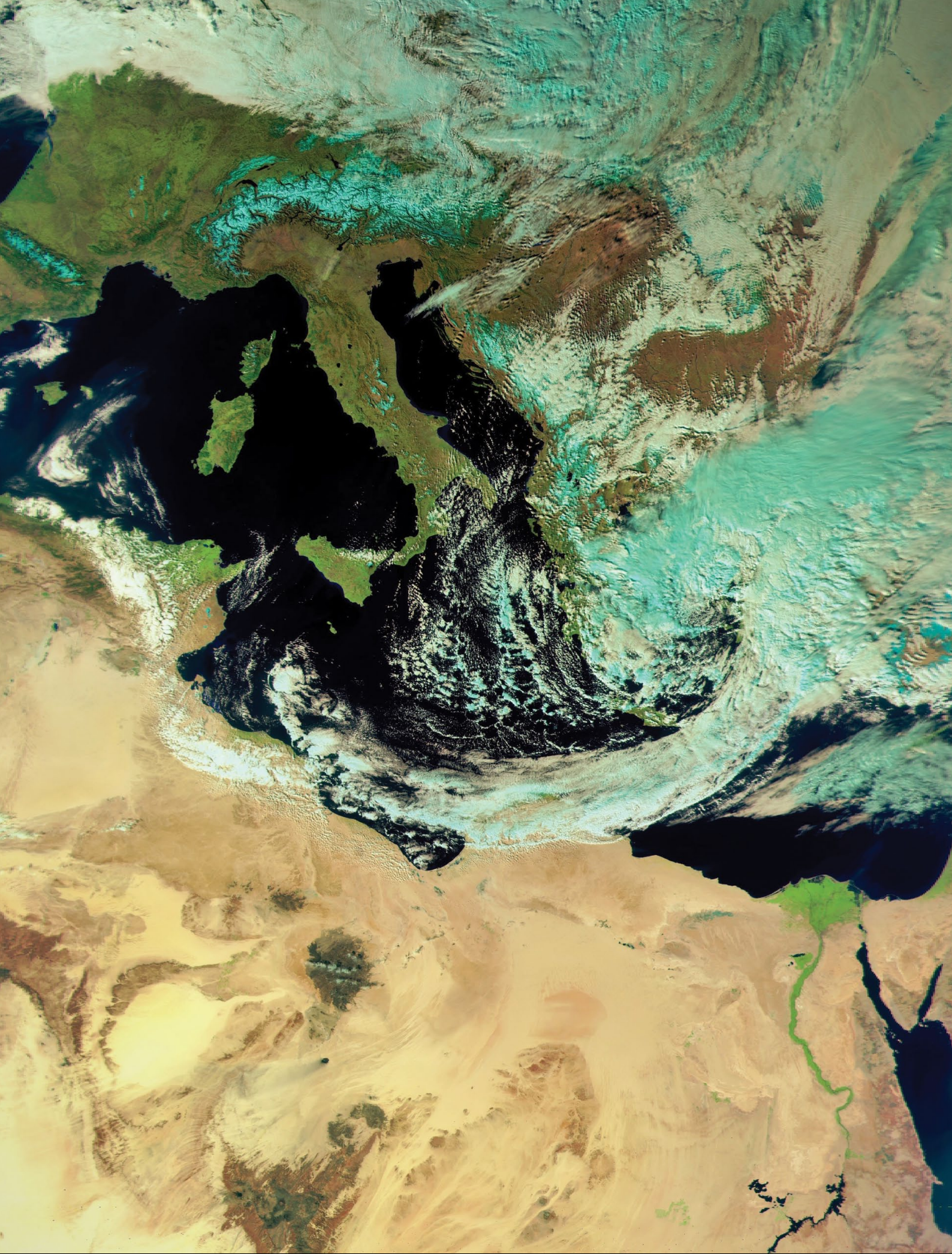

This splendid RGB123 AHRPT image from Meteor M2 was acquired by Enrico Gobbetti on February 8, 2022, showing clearly his native Italy basking in sunshine. The alps to the north render as cyan, confirming their blanket of winter snow.

A View of Vesuvius

NASA Earth Observatory

Story by Sara E. Pratt

NASA Earth Observatory image by Joshua Stevens, using Landsat data from the U.S. Geological Survey.

Mount Vesuvius, located 12 kilometers (7.5 miles) southeast of Naples, Italy, is the only active volcano on Europe's mainland. It is a composite stratovolcano, made up of pyroclastic flows, lava flows, and debris from lahars that accumulated to form the volcanic cone.

In this natural-color image, acquired on January 2, 2022, by the Operational Land Imager (OLI) on Landsat 8, the cone of Mount Vesuvius appears through a break in the clouds. The ridge surrounding the cone is a remnant of the collapsed caldera of an older volcano, Mount Somma, from which the cone of Vesuvius emerged.

Naples has a population of 3 million people, 800,000 of whom live on the volcano's slopes. This makes Vesuvius one of the most dangerous volcanoes on the planet. Its most famous eruption, in A.D. 79, destroyed the cities of Pompeii and Herculaneum. The cities were engulfed in pyroclastic flows—superheated, high-density clouds of volcanic gas, ash, and rock that flow downslope at hundreds of kilometers per hour. Pliny the Younger's eyewitness account of that eruption, including its towering ash cloud, led volcanologists to term these types of eruptions "Vesuvian" or "Plinian."

Such catastrophes are why the area became home to the world's first volcanological observatory, built in the 19th century. Today, Vesuvius remains one of the most heavily monitored and studied volcanoes in the world. By dating lavas, scientists know that the mountain has had eight major eruptions in the past 17,000 years. The most recent, on March 17, 1944, destroyed the village of San Sebastiano, Italy. Since then, the volcano has experienced occasional earthquake activity, ground deformation, and gas venting from the crater.

Visualising EUMETCast SAF products: part 2

Richard Osborne

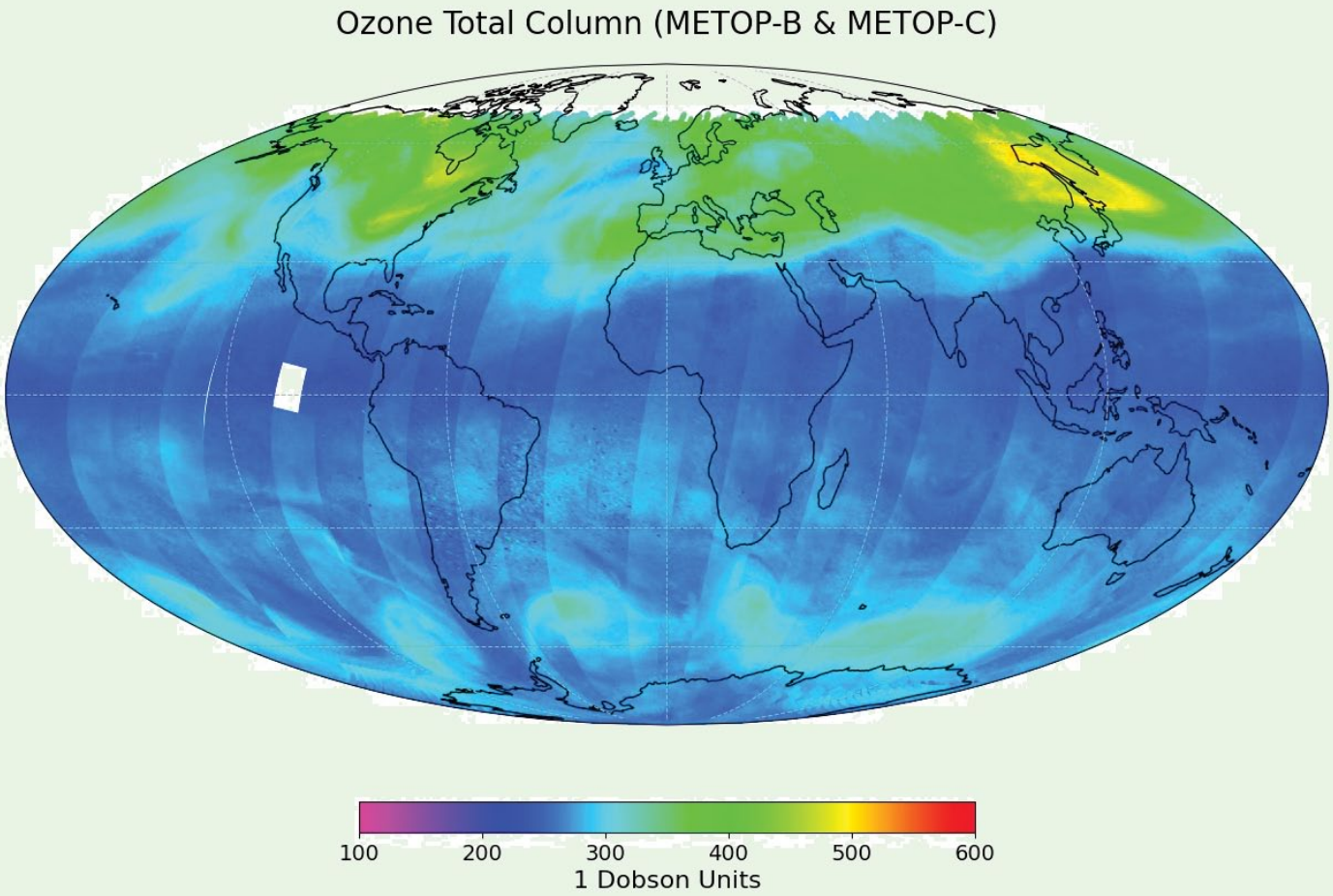

Ozone Total Column on Mollweide Projection showing high levels over Eastern China.

Introduction

In the December 2021 edition of the GEO Newsletter, I presented an article about visualising EUMETCast Satellite Applications Facilities (SAF) products. At the time of publication, I declared that my work on the Atmospheric Composition (AC) products was very much a work in progress as I had only just started to look at the implementation in detail. I am now able to provide an update on my efforts so far.

Atmospheric Composition (AC)

Over EUMETCast, the AC SAF disseminates data for Aerosol Absorbing Index (AAI), Absorbing Aerosol Height (AAH) and trace atmospheric gases; namely ozone, nitrogen dioxide (two products), sulphur dioxide and formaldehyde. The primary distribution format is HDF5 files with BUFR files in a secondary role. I concentrated on the former as BUFRDisplay takes care of the latter. Two satellites currently provide the data from their GOME-2 instrument: MetOp-B and MetOp-C.

Looking in detail at the format of the HDF5 files, the AAI and AAH products have a two dimensional data structure with full geo-referencing, albeit in a complex format. In addition, these products are delivered in chunks as a sequence of files, each containing three minutes worth of data.

The trace atmospheric gas data is also delivered in chunks as a sequence of files, each containing up to three minutes worth of data (but it could be less). Each chunk contains the data for all the represented gases and this is represented in the file name. In contrast to the AAI and AAH products however, the trace gas files have a one dimensional data structure, possibly because of their variable length. They also include full geo-referencing in a complex format.

As stated in the original article, the format of the HDF5 files, coupled with the need to combine data from multiple files to produce a global image, means that only general purpose or bespoke software can provide a satisfactory method of visualising the data. Following a period of research, I located some candidate *Python* scripts on a EUMETSAT software repository at

https://gitlab.eumetsat.int/eumetlab/atmosphere/atmosphere

and used these as the basis for my experiments.

Text continues on page 37

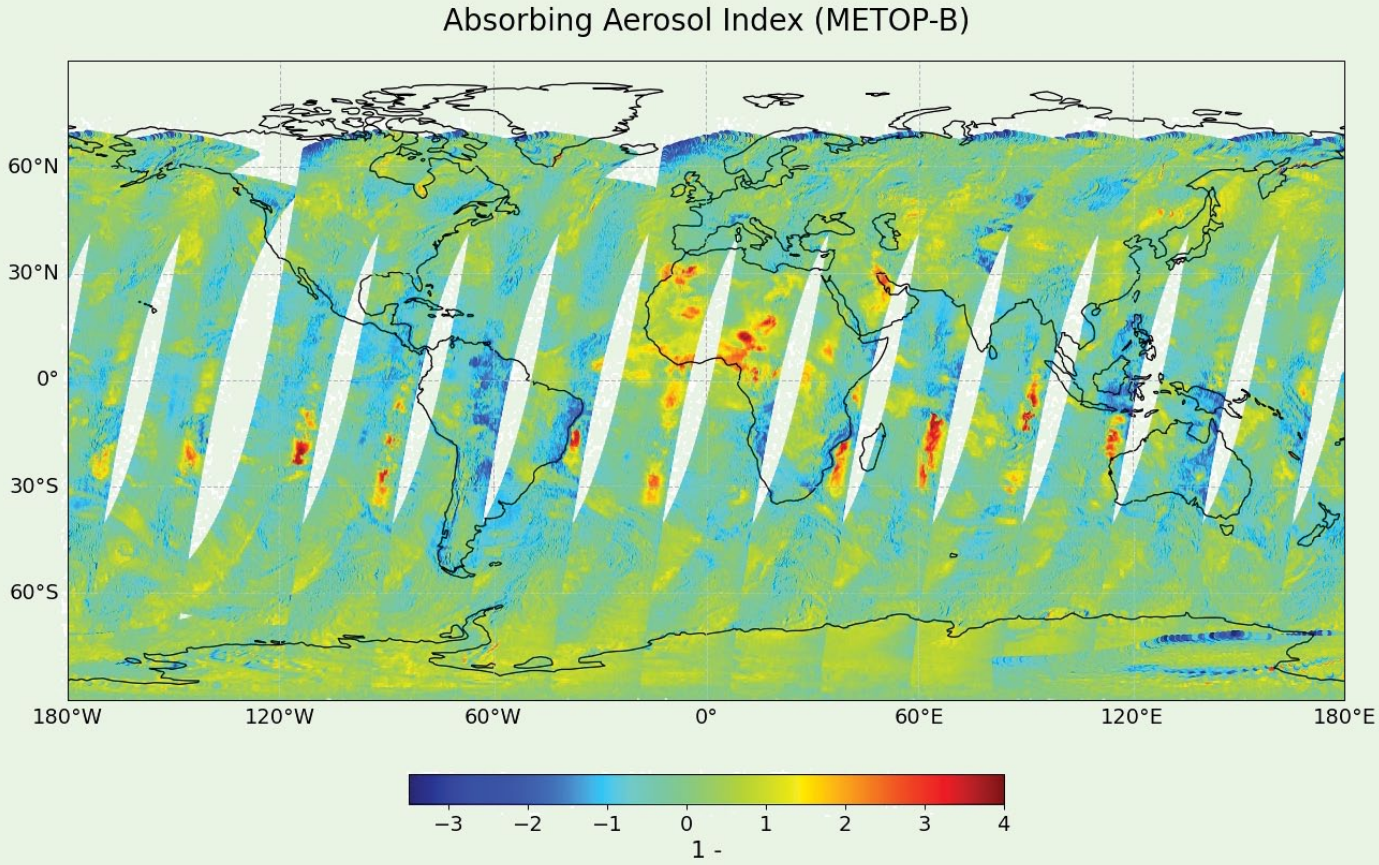

Aerosol Index derived from METOP-B on Plate Carree Projection. Positive values are absorbing, negative values are scattering.

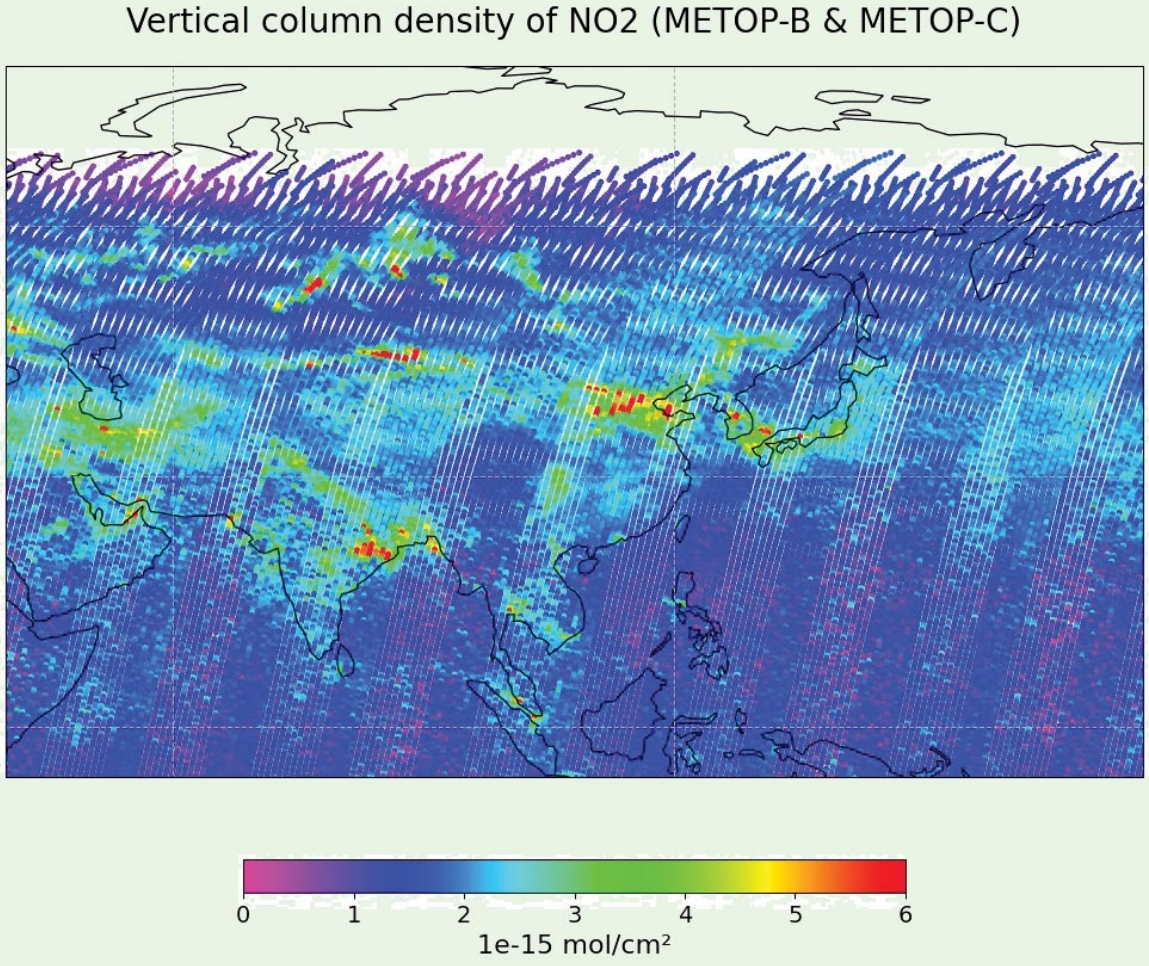

Nitrogen Dioxide density over Asia showing hotspots on Plate Carree Projection.
Image quality is denser where MetOp-B and MetOp-C scans overlap.

AC Scripts

After consulting the AC SAF website for information on each of the products and the software repository, I elected to ignore AAH and concentrate on the remainder. As the aerosol and each of the trace gases requires a different treatment to produce the best visual image, I decided to produce a series of individual *Python* scripts resulting in a total of six top level scripts and an additional one containing common functions. However, the workflow is the same for all the top level scripts and can be summarised as follows:

- Extract relevant data from all available HDF5 files and combine into a single data array using *Python* Xarray module.
- Filter data array using Xarray to remove or correct extraneous values.
- Plot data onto a basemap using *Python Matplotlib* and Cartopy modules adding a colourmap legend.

When calling each *Python* script, I include two arguments in the command line. The first selects the satellite data for viewing: MetOp-B, MetOp-C or both. The second selects the map projection such as Plate Carrée, Mollweide or Orthographic. For ease of use, I prepared a simple Windows batch file to construct the required command line, based on a series of multiple choice questions which asks for the desired product, satellite(s) and projection.

When I produced my first global plots they didn't look right, so I investigated further. I discovered that the observation data for the aerosols and gases includes the output from two separate scans, each covering the same ground area. The GOME-2 instrument provides an initial forward scan and then a lower resolution backward scan and I was plotting one on top of the other. This fact is not mentioned in the EUMETSAT sample scripts but I did find a way to remove the backward scan contribution from the data array to produce a 'clean' plot. Examples of the plots are shown above. To define the measurement range for each product and check that the plotted data looked correct, I referred to two AC SAF related websites which provided representative images [1,2], and was gratified to observe that they correlated very closely.

The Atmospheric Composition was the most challenging SAF product for me to visualise as it relies on a pure *Python* solution supported by powerful modules such as *Xarray*, *MatPlotlib* and *Cartopy*. Unfortunately, as someone who just dabbles on the edge of programming, I found the documentation for these packages to be arcane and almost impenetrable, making progress very difficult. Even the act of adding an additional colour map to *Matploblib* proved to be difficult.

Commentary

I believe that I have succeeded in my original quest to visualise as many EUMETCast SAF products as possible although it took several different methods ranging from instant 'point and click' solutions to bespoke *Python* scripts. I'm sure that there are other methods that would produce equivalent results but I simply used those that I could find at the time.

On the assumption that I haven't missed any readily available 'off the shelf' software applications I think that *Python* solutions offer the best scope for further self-experimentation. For example, there is a visualisation package for derived meteorological products in BUFR, netCDF and GRIB format called *Magics* from the European Centre for Medium-Range Forecasts that looks similar to *Pytroll/Satpy* in concept. Maybe I'll give it a try.

Postscript

As started at the beginning of Part 1, my objective was to provide an overview of my experiments to visualise EUMETCast SAF products and the article has been presented at a 'high level' with very little detail. However, if any reader would like more information, including sample scripts, I will respond to requests placed on the MSG-1 Groups website at

https://groups.io/g/MSG-1

References

1 GOME-2 Vertical Ozone Profiles and Absorbing Aerosol Index
https://www.temis.nl/acsaf/?sat=metopb

2 GOME-2 / MetOp
https://atmos.eoc.dlr.de/app/missions/gome2

Antarctic Eclipse

On December 4, 2021, a handful of people in Antarctica were treated to clear views of a total solar eclipse, the only one to occur in 2021. This image was acquired by the **Earth Polychromatic Imaging Camera** (EPIC) aboard the Deep Space Climate Observatory (DSCVR) from its position at Lagrange Point 1, a gravitationally stable point between the Sun and Earth about 1.5 million kilometres from Earth. In this view, acquired at 07:58 UTC, the Moon's shadow can be seen falling on Antarctica.

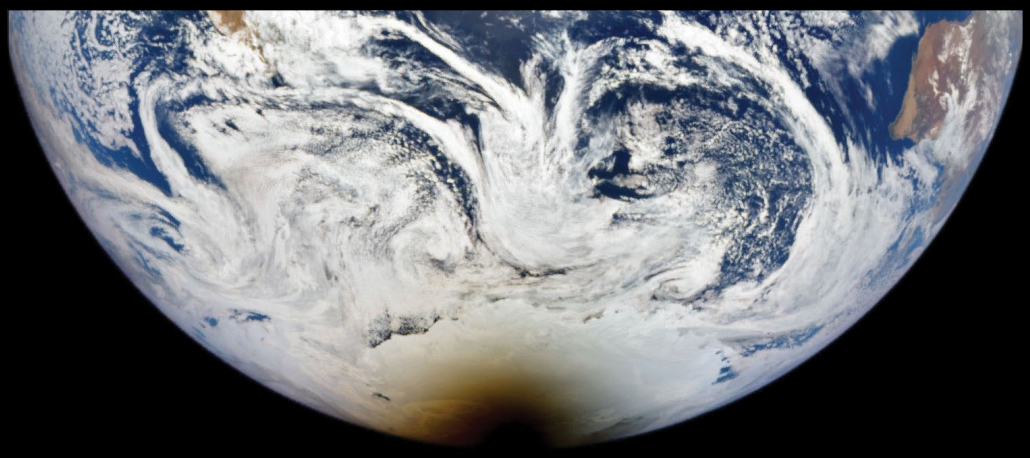

NASA image courtesy of the DSCOVR EPIC team

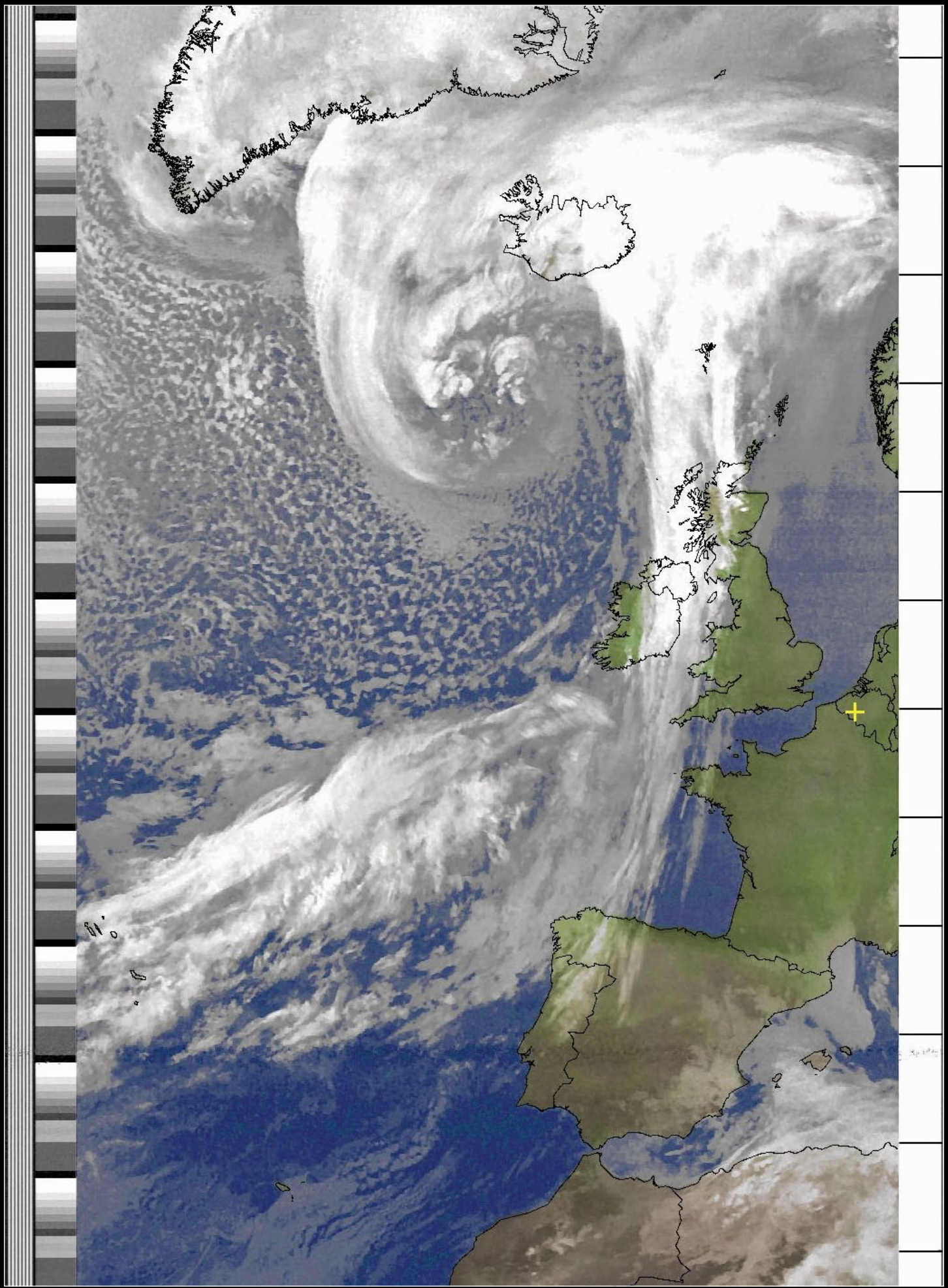

This striking NOAA 18 APT image, sent in by André T'Kindt from Ronse in Belgium, shows a deep depression over Iceland driving blustery winds and rain showers across Great Britain on February 27, 2022.

Bahamas

MODIS Web Image of the Day

https://modis.gsfc.nasa.gov/gallery/showall.php

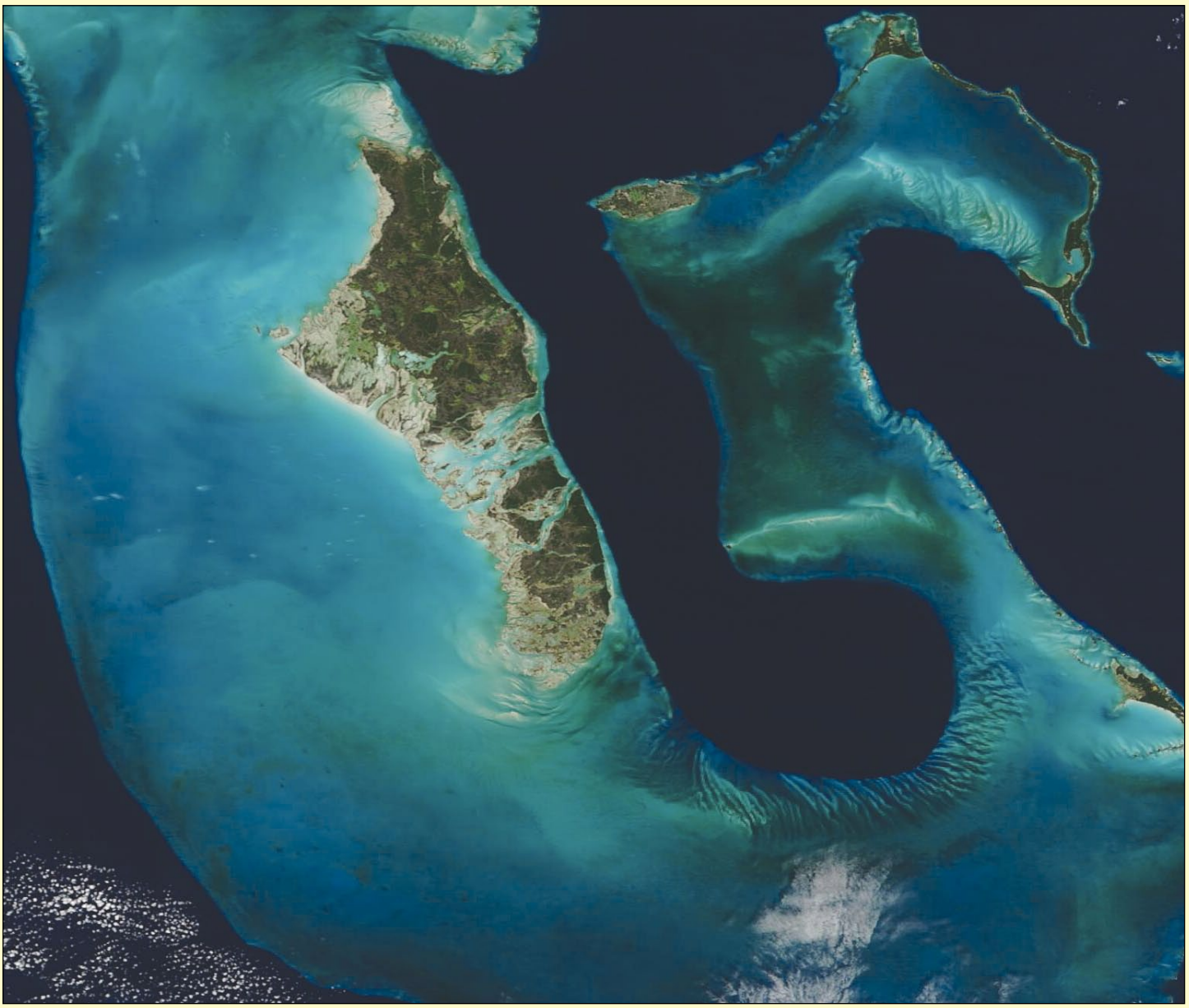

Image Credit: MODIS Land Rapid Response Team, NASA GSFC

This stunning true-colour image of a portion of the Bahamas was acquired by the Moderate Resolution Imaging Spectroradiometer (MODIS) on board NASA's Terra satellite on December 16, 2021. The sparkling-clear sky allows a detailed view of Andros Island in the west, Eleuthera Island in the east, the bright jewel-tones of the Great Bahama Bank and the intense blue of a deep underwater canyon that separates Andros Island from Eleuthera.

The largest island of the Bahamas, Andros measures about 160 kilometres in length by 70 km in width. The flat, forested island is actually a conglomeration of multiple islands which are strung together by a series of wetlands. To the west, the waters over the limestone-rich mound known as the Great Bahama Banks are extremely shallow—in some areas, under one metre at most. Limestone is a sedimentary rock formed by the skeletal fragments of sea creatures, including corals and foraminifera, and this particular limestone platform has been accumulating since at least the Cretaceous Period.

To the east of Andros, the sea floor abruptly plunges downward, reaching a depth of about 4300 metres. This deep water appears very dark, in brilliant contrast to the light colour of the shallowest areas of the Great Bahamas Bank. The submarine trench appears to take the shape of a long tongue, giving this unique feature the name of '*Tongue of the Ocean*'. Colourful wave-shaped ripples sit at the southern edge of the Tongue. These are large underwater dunes that have been shaped by the action of the waves over time.

Lake Erie's February Freeze

MODIS Web Image of the Day

https://modis.gsfc.nasa.gov/gallery/showall.php

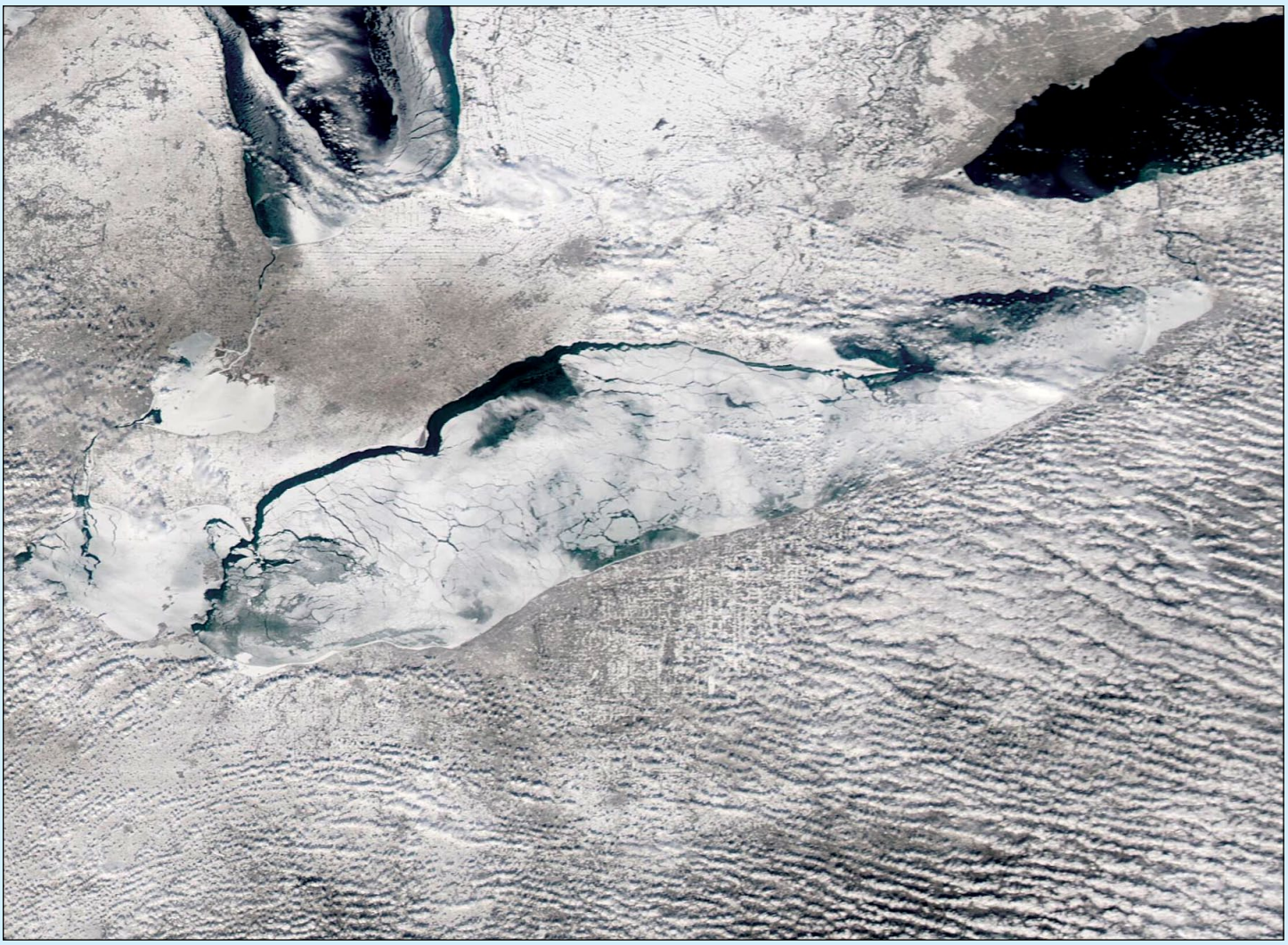

Image Credit: MODIS Land Rapid Response Team, NASA GSFC

Each year, frigid winter chill brings a topping of ice to the Great Lakes while wicked winter winds force thin ice to shift, breaking it up, and expanding the extent of open water. These wintery dynamics create a sort of dance across the largest lakes in North America, with ice growing and retreating based primarily on variations in wind and air temperature.

Since January 2022, the ice cover on Lake Erie has proven a case in point. In late January, Lake Erie almost entirely froze over, with ice cover growing well beyond the seasonal average to reach 94%. By February 3, the ice cover had dropped to about 62% before rising again to 90% by February 5. Another steep drop in ice occurred after that, with ice cover falling to about 55% on February 11 only to shoot back up to about 72% on February 14.

As the shallowest of the Great Lakes, Erie has the highest annual maximum ice cover, regularly reaching more than 80%. Three times in the past half century, Lake Erie reached 100% ice cover: in 1978, 1979, and 1996. Conditions on the lake are not only highly variable from year to year, but also from day to day. The first week of February 2022 brought a heavy snowstorm, wildly varying wind speeds and directions, and days of continuous cooling. As a result, the ice extent across the Great Lakes rapidly expanded. On February 1, the average ice cover across all the lakes was 12%; two days later it had expanded to 28% and by February 6 it was 43%. (Between 1973–2021, the Great Lakes' annual average maximum ice coverage was 53.1 percent.)

The Moderate Resolution Imaging Spectroradiometer (MODIS) on board NASA's Aqua satellite acquired this true-colour image of Lake Erie on February 14, 2022. Surrounded by snow and cloud, the lake was almost completely covered with ice, except for areas near the northern coasts where open water prevailed. Ice also covered much of the southern tip of Lake Huron while most of the western section of Lake Ontario remained ice-free.

Garabogazköl Basin

MODIS Web Image of the Day

https://modis.gsfc.nasa.gov/gallery/showall.php

Pale shades of teal, turquoise, tan, and salty white filled the waters of the Garabogazköl Depression in this stunning true-color image, which was acquired by the Moderate Resolution Imaging Spectroradiometer (MODIS) on board NASA's Terra satellite on November 19, 2021.

Also known as the Zaliv Kara-Bogaz-Gol, Garabogazköl Gulf, and Garabogazköl Bay, the extremely salty and shallow basin sits in an arid location in Turkmenistan. The Garabogazköl Basin was once relatively well-connected to the dark waters of the Caspian Sea, allowing water fresh water to flow freely into the basin. Drought and diversion of water from the major rivers that feed the Caspian Sea (the Volga and Kur Rivers) caused the level of the Sea waters to lower, slowing the freshwater intrusion into the Garabogazköl. In 1980, a dam was completed which completely blocked the connection between the Caspian and the basin, creating rapid evaporation which reduced that Garabogazköl to about 1/3 of its former size and dropped the average depth to less than 50 cm (19.5 inches). The dam was destroyed in 1992 and today the Caspian Sea and the Garabogazköl share a narrow connection that allows survival of the water in the shallow basin.

Image Credit: MODIS Land Rapid Response Team, NASA GSFC

Water in Uyuni Salt Pan

MODIS Web Image of the Day

https://modis.gsfc.nasa.gov/gallery/showall.php

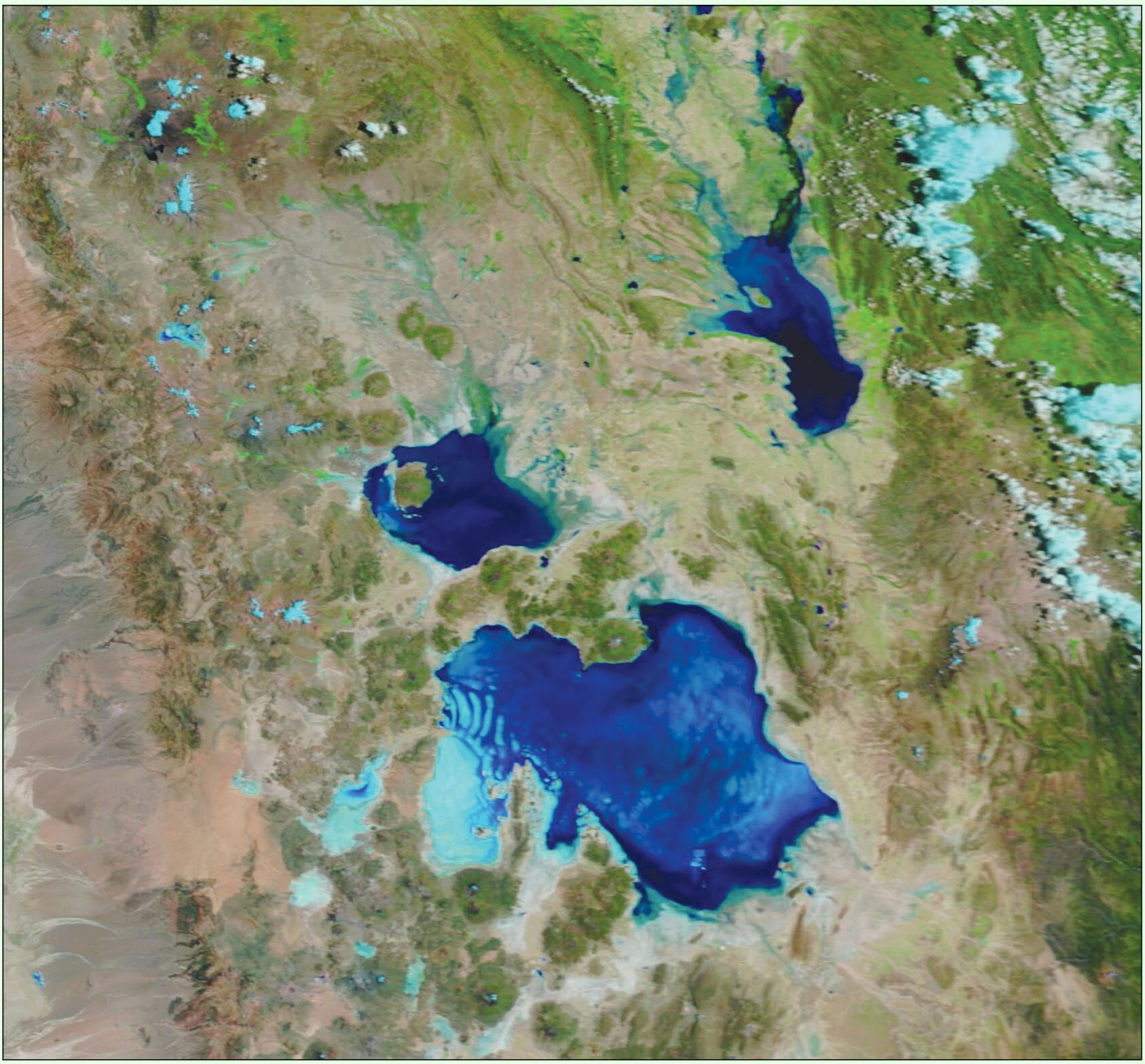

Image Credit: MODIS Land Rapid Response Team, NASA GSFC

Sitting in the high Altiplano of Bolivia, the Salar de Uyuni is the largest playa (salt flat) on Earth. Covering an expanse of 10,582 square kilometres, which is roughly the size as the 'Big Island' island of Hawaii, the salar is covered with a mineral crust and typically looks bright white from space, especially during the dry season (May to November). Even though the Salar de Uyuni and the smaller Salar de Coipasa—which sits to Uyuni's northwest—receive less than 200 millimetres of rain each year, the rainy season brings tremendous change. Often, the mineral crust of the salt flats will become covered with water, creating a mirror-like effect when viewed from Earth—a spectacular site adored by tourists.

On February 11, 2022, the Moderate Resolution Imaging Spectroradiometer (MODIS) on board NASA's Terra satellite acquired a beautiful false-colour image of Salar de Uyuni, the Salar de Coipasa, and Lake Poopo. This particular false colour image uses infrared and visible light (bands 7,2,1), a combination that aids in separating water (deep blue) from vegetation (bright green), cloud (white or pale blue) and open land (tan). Lakes covered with mineral salts appear electric blue. As salt becomes wetter, it takes on a darker tone. This image makes it clear that all three salt flats contain copious water in early February, which is approaching the end of the rainy season.

Iceberg B-22A

MODIS Web Image of the Day

https://modis.gsfc.nasa.gov/gallery/showall.php

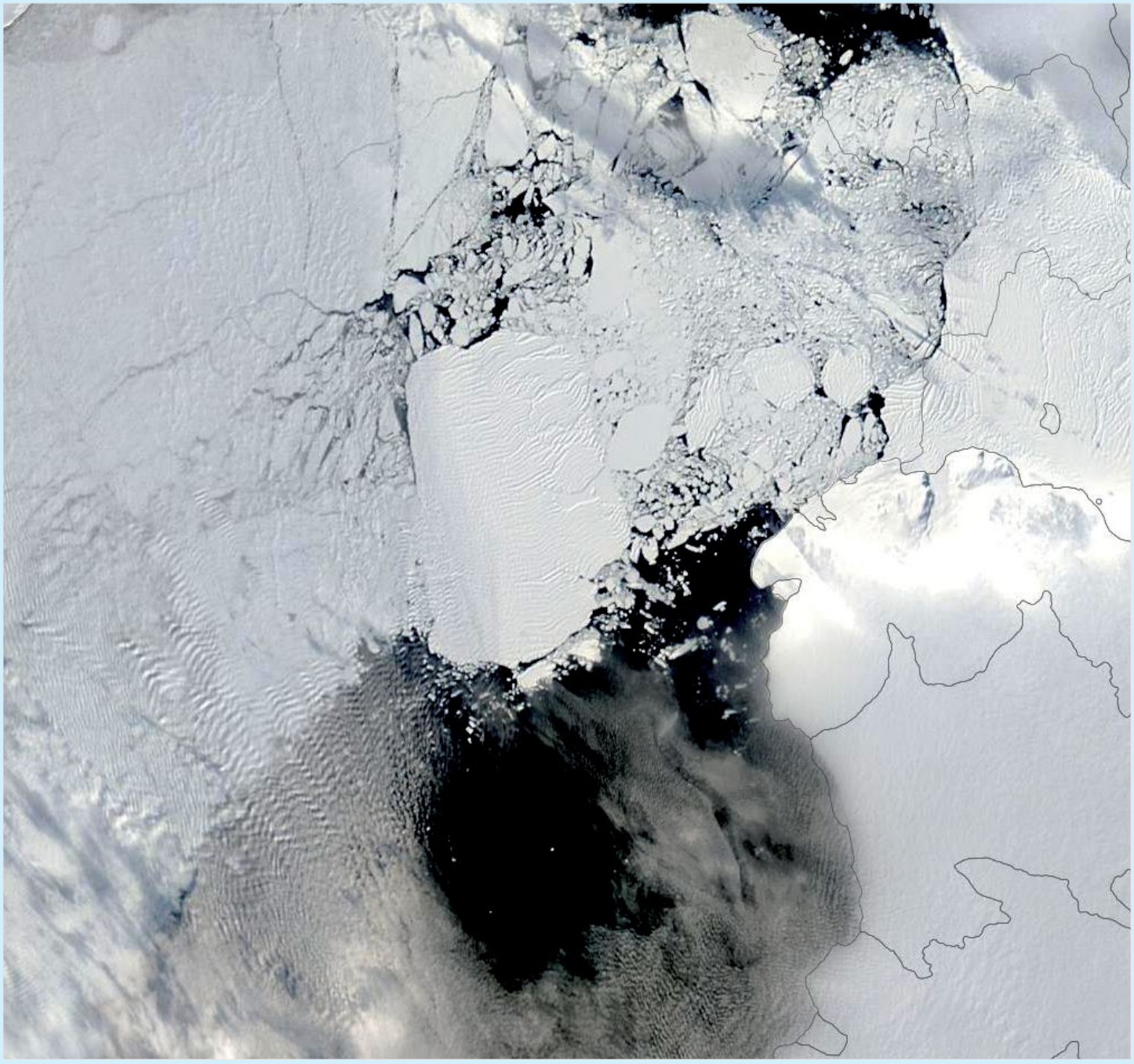

Image Credit: MODIS Land Rapid Response Team, NASA GSFC

Almost twenty years ago, in mid-March 2002, a massive Antarctic iceberg broke off the ice tongue of the Thwaites Glacier and slowly inched its way into Pine Island Bay, part of the Amundsen Sea.

Shortly after calving, four fragments broke off the almost-Delaware-sized iceberg. Caught by currents, the smaller fragments drifted away but the large iceberg, dubbed B-22A, grounded not far from the mother tongue.

As of February 18, 2022, iceberg B-22A has drifted only 53 kilometres—a remarkably slow crawl of about 2.6 kilometres per year. The berg initially measured 85 by 65 kilometres. The *U.S. National Ice Center* reported that, as of February 18, the 'berg measured 70.3 by 44.4 kilometres. That same day, B-22A was spied sitting in the Amundsen Sea by the Terra satellite's Moderate Resolution Imaging Spectroradiometer (MODIS), which captured this true-colour image to give a beautiful view of the iceberg at one point in time.

Currently Active Satellites and Frequencies

Polar APT/LRPT Satellites			
Satellite	Frequency	Status	Image Quality
NOAA 15	137.6200 MHz	On	Good
NOAA 18	137.9125 MHz	On	Good
NOAA 19	137.1000 MHz	On	Good [1]
Meteor M N1	137.0968 MHz	Off	Dead [8]
Meteor M N2	137.1000 MHz	On	Good
Meteor M N2-2	137.9000 MHz	Off	System failure [12]

Polar HRPT/AHRPT Satellites				
Satellite	Frequency	Mode	Format	Image Quality
NOAA 15	1702.5 MHz	Omni	HRPT	Weak
NOAA 18	1707.0 MHz	RHCP	HRPT	Good
NOAA 19	1698.0 MHz	RHCP	HRPT	Good
Feng Yun 1D	1700.4 MHz	RHCP	CHRPT	None: Device failure
Feng Yun 3A	1704.5 MHz	RHCP	AHRPT	Inactive [2,10]
Feng Yun 3B	1704.5 MHz	RHCP	AHRPT	Active [2]
Feng Yun 3C	1701.4 MHz	RHCP	AHRPT	Active [2]
Metop B	1701.3 MHz	RHCP	AHRPT	Good
Metop C	1701.3 MHz	RHCP	AHRPT	Good
Meteor M N1	1700.00 MHz	RHCP	AHRPT	Dead [8]
Meteor M N2	1700.0 MHz	RHCP	AHRPT	Good
Meteor M N2-2	1700.0 MHz	RHCP	AHRPT	Active [12]

Geostationary Satellites				
Satellite	Transmission Mode(s)		Position	Status
Meteosat 8	HRIT (digital)	LRIT (digital)	41.5°E	IODC
Meteosat 9	HRIT (digital)	LRIT (digital)	3.5°E	On [5]
Meteosat 10	HRIT (digital)	LRIT (digital)	9.5°E	Off [4]
Meteosat 11	HRIT (digital)	LRIT (digital)	0°W	On [3]
GOES-13	GVAR 1685.7 MHz	LRIT 1691.0 MHz	60°W	Off
GOES-14	GVAR 1685.7 MHz	LRIT 1691.0 MHz	105°W	Standby
GOES-15 (W)	GVAR 1685.7 MHz	LRIT 1691.0 MHz	128°W	On [6]
GOES-16 (E)	GRB 1686.6 MHz	HRIT 1694.1 MHz	75.2°W	On[6,9]
GOES-17	GRB 1686.6 MHz	HRIT 1694.1 MHz	137.2°W	[11]
MTSAT-1R	HRIT 1687.1 MHz	LRIT 1691.0 MHz	140°E	Standby
MTSAT-2	HRIT 1687.1 MHz	LRIT 1691.0 MHz	145°E	On
Feng Yun 2D	SVISSR	LRIT	123.5°E	Backup/Off [7]
Feng Yun 2E	SVISSR	LRIT	86.5°E	On
Feng Yun 2F	SVISSR	LRIT	112.5°E	Standby
Feng Yun 2G	SVISSR	LRIT	99.5°E	On
Feng Yun 2H	SVISSR	LRIT	86.5²E	
Feng Yun 4A	HRIT (digital)	LRIT (digital)	99.5°E	On

Notes

1 LRPT Signals from Meteor M N2 may cause interference to NOAA 19 transmissions when the two footprints overlap.
2 These satellites employ a non-standard AHRPT format and cannot be received with conventional receiving equipment.
3. Meteosat prime Full Earth Scan (FES) satellite
4 Meteosat backup Full Earth Scan (FES) satellite
5 Meteosat prime Rapid Scanning Service (RSS) satellite.
6 GOES 15 also transmits EMWIN on 1692.700 MHz
GOES 16 also transmits EMWIN on 1694.100 MHz
GOES 17 also transmits EMWIN
7 There has been no imagery from Feng Yun 2D since June 30, 2015. Since Feng Yun 2G is operating from the same position (86.5°E), it is likely that FY-2D is now in standby as a backup satellite.
8 On March 20, 2016, Meteor M1 suffered a catastrophic attitude loss, frequently pointing its sensors towards the sun. The following day all signals ceased and it seems highly probable that this satellite is now incapable of imaging the Earth.
9 GOES Rebroadcast (GRB) provides the primary relay of full resolution, calibrated, near-real-time direct broadcast space relay of Level 1b data from each instrument and Level 2 data from the Geostationary Lightning Mapper (GLM). GRB replaces the GOES VARiable (GVAR) service.
10 Although Feng Yun 3A's status is recorded on the wmo-sat website as 'inactive (end of operation)', it continues (as of June 2018) to transmit imagery.
11 GOES 17 is expected to start operations during January 2019.
12 Following a collision with a micrometeorite, the power system aboard Meteor M2-2 has been compromised. AHRPT is still being transmitted when the solar panels are sunlit, but there is insufficient battery power to enable the LRPT stream..